Eur. Phys. J. Spec. Top. (2025) 234:3357–3374
https://doi.org/10.1140/epjs/s11734-025-01687-9

THE EUROPEAN PHYSICAL JOURNAL SPECIAL TOPICS

Regular Article

On the shifts of orbits under perturbation and the change of full-period Jacobian of periodic orbits

Wenyin Wei[1,2,3], Alexander Knieps[3], Jiankun Hua[3,4], and Yunfeng Liang[1,3,a]

[1] Institute of Plasma Physics, Hefei Institutes of Physical Science, Chinese Academy of Sciences, Hefei 230031, People's Republic of China
[2] University of Science and Technology of China, Hefei 230031, People's Republic of China
[3] Forschungszentrum Jülich GmbH, Institute of Fusion Energy and Nuclear Waste Management-Plasma Physics, Jülich 52425, Germany
[4] International Joint Research Laboratory of Magnetic Confinement Fusion and Plasma Physics, State Key Laboratory of Advanced Electromagnetic Engineering and Technology, School of Electrical and Electronic Engineering, Huazhong University of Science and Technology, Wuhan 430074, People's Republic of China

Received 6 January 2025 / Accepted 12 May 2025 / Published online 13 August 2025

Abstract Periodic orbits and cycles play essential roles in discrete- and continuous-time dynamical systems (i.e., maps and flows), respectively. To succinctly describe their shifts when the system is applied perturbation, the concepts of functional and functional derivative from functional analysis are employed to treat the entire system as an argument of the geometric object representation such as a trajectory or a flux surface. For example, a trajectory initiating from $\boldsymbol{x}_0$ after time t is now denoted by $\boldsymbol{X}[\mathcal{B}](\boldsymbol{x}_0, t)$ with the vector field $\mathcal{B}$ explicitly stated as an argument. The resulting shifts of an orbit/trajectory and periodic orbit/cycle are analyzed and concluded as explicit formulae for maps/flows, respectively. These formulae form the foundation of Functional Perturbation Theory (FPT), which facilitates the analysis of sensitivity to perturbations and the optimization or control of various systems. Leveraging FPT in dynamical systems enables one to efficiently *a priori* estimate the shifts of cycles, which serve as the structural skeleton of the system. If an unfavorable perturbation is known *a priori*, an opposing perturbation or a combination of alternative perturbations can be employed to counteract its adverse effects. These calculations can now be completed within seconds, even without specialized hardware acceleration. The primary motivation for developing FPT is to weaken the plasma-wall interaction in a divertor configuration of magnetic confinement plasmas, which in turn can be considered one of the most economically valuable applications of FPT: facilitate plasma detachment by tuning the parallelism of nearby field-line trajectories to the divertor X-cycle(s) through the full-period Jacobian $\mathcal{DP}^m$ of field-line tracing at the divertor X-cycle(s). The closer the eigenvalues of $\mathcal{DP}^m$ are to unity, the longer the field-line connection lengths become, serving as a direct indicator of a favorable divertor configuration. The power entering the scrape-off layer can be effectively dissipated via the extended field-line connection length. Notably, the technique of employing functionals extends beyond field-line tracing in magnetic confinement fusion and is applicable to a broader range of ODE (ordinary differential equation) systems, as it deeply integrates ODE theory with the method of variation. The formulae are deliberately presented in a general form to facilitate the application of FPT across various academic domains.

1 Introduction

This paper presents a theory addressing the *shifts of orbits, particularly those periodic ones, under perturbation*, driven by practical demands for optimizing and controlling three-dimensional (3D, i.e., non-axisymmetric) magnetic fields in magnetically confined fusion (MCF) devices. The theory even extends to arbitrary finite-dimensional dynamical systems governed by ordinary differential equations (ODEs), as it is found during derivation that neither the dimensionality constraint nor the vanishing divergence condition is essential for maintaining its validity and conciseness. Generalization to infinite-dimensional dynamical systems [1] generated by partial differential

[a] e-mail: y.liang@fz-juelich.de (corresponding author)

equations (PDEs) is possible but requires more effort beyond this paper, which can offer a convenient computational method to estimate the sensitivity of the system to the initial conditions.

In the MCF community, efforts [2–10] to mitigate or suppress Edge Localized Modes (ELMs) in tokamak plasmas involves introducing external Resonant Magnetic Perturbations (RMPs) to let island chains grow and corrode each other, then a chaotic field is created, in which magnetic field-line tracing exhibits an ergodic characteristic that orbits in the chaotic regions appear irregular, in contrast to the regular orbits that form tori. The resulting chaotic field enhances effective radial transport, thereby reducing the transient heat flux peak released by ELMs, as the edge pressure gradient is prevented from accumulating to unacceptable levels. However, the classical theories[11–14] underlying this approach have inherent limitations due to relying on Fourier analysis of the radial magnetic perturbation $B^r = \boldsymbol{B} \cdot \nabla r$ in the flux coordinates (r, θ, φ) or its equivalents that require the integrability of the perturbed system. The chaotic field expanded by the stable and unstable manifolds of the outermost X-cycle(s) is probably the largest one in MCF machines [15], yet can be ignored because $r = 1$ is a singularity for these coordinate systems, prompting a return to the standard cylindrical coordinates to avoid errors induced by transforming to flux coordinates and back.

The chaotic field is not unique in toroidal magnetic fields but is common in autonomous continuous-time systems of three dimensions or more, not necessarily divergence-free. Chaos in 2D continuous-time systems is forbidden by Poincaré-Bendixson theorem. For discrete-time systems, one dimension is sufficient to allow chaos to exist.

Functional Perturbation Theory (FPT) is a framework developed in this work to systematically analyze how orbits, particularly those periodic ones, shift under global perturbations to the dynamical system. FPT enables explicit and analytical derivation of these shifts by treating the entire system as an argument of geometric object representations such as that of a trajectory. The theory leverages functional derivatives to provide a quantitative understanding of perturbation-induced changes.

Functional—a function of function—is not a novel concept introduced to physicists from mathematics. In quantum physics, it is common practice to write various forms of energy as functions of the electronic wave function ψ, which has established a systematic framework of density functional theory (DFT). In contrast, in this paper, by considering the entire system as an argument of orbits, the *Functional Perturbation Theory* (FPT) significantly enhances one's ability to analyze the change of these geometric objects under perturbation. The FPT can be a bit more complicated than DFT due to the more complex composite relationships between functions. Nonetheless, for computers, these ODE systems can be solved within seconds on an economical laptop using Julia for a stellarator, as the essence of magnetic topology is distilled and decoupled from complicated plasma dynamics. This efficiency ensures that actuators in future MCF machines can respond in real-time. Notably, in the fully axisymmetric case of tokamaks, these formulae can simplify significantly, further reducing computational demands and enhancing practical applicability.

Beyond MCF, this theory finds broad application in analyzing dynamical systems [16–24] and the island-around-island structures of chaotic fields [25–27]. In aerospace dynamics [28–30], trajectories like halo orbits and libration point paths are highly sensitive to perturbations, making them challenging to maintain precisely. By integrating this theory with spacecraft propulsion systems through automated control, deviations from these delicate paths can be effectively corrected, ensuring robust operation even under external influences.

2 Fundamental equations and notations

This section merely provides foundational techniques as disciplinary background, whereas the derivation of FPT begins in Sect. 3.

For a general N-D dynamical system,

$$\frac{\partial}{\partial t}\boldsymbol{X}(\boldsymbol{x}_0, t) = \boldsymbol{B}(\boldsymbol{X}) = \begin{bmatrix} B_1(\boldsymbol{X}) \\ B_2(\boldsymbol{X}) \\ B_3(\boldsymbol{X}) \\ \vdots \\ B_{N-1}(\boldsymbol{X}) \\ B_N(\boldsymbol{X}) \end{bmatrix}, \quad \begin{array}{c}(\text{where } B_i \text{ is simply} \\ \text{the expression for the } i\text{th} \\ \text{ODE of the system.})\end{array} \tag{1a}$$

and a 3D toroidal vector field as a special case of the former when $N = 3$ and expressed in cylindrical coordinates,

$$\frac{\partial}{\partial \phi_e}\boldsymbol{X}_{\text{pol}}(\boldsymbol{x}_{0,\text{pol}}, \phi_\text{s}, \phi_\text{e}) = \frac{R\boldsymbol{B}_{\text{pol}}}{B_\phi}(\boldsymbol{X}_{\text{pol}}, \phi_\text{e}), \tag{1b}$$

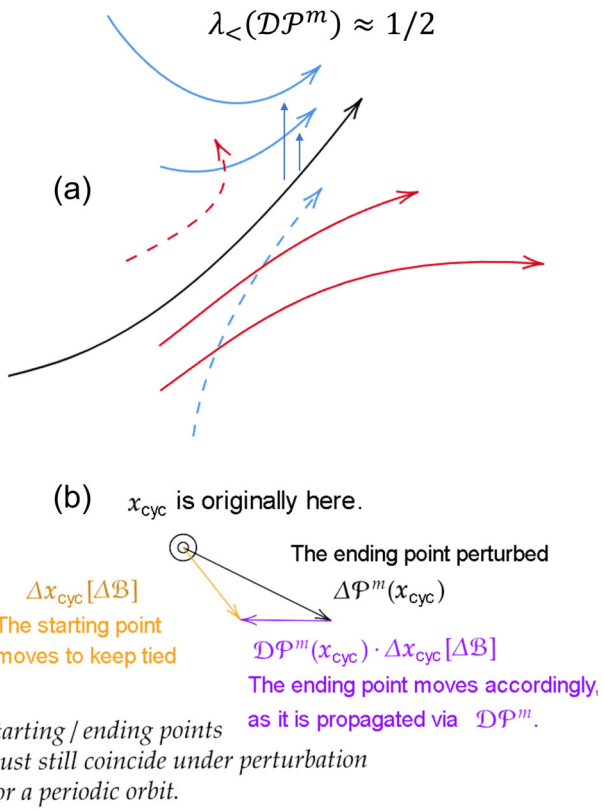

Fig. 1 (**a**) Cartoon illustrating the geometric significance of $\mathcal{D}\mathcal{P}^m$: *its eigenvalues and eigenvectors dictate the rates of convergence or divergence of nearby trajectories and the directions in which they occur*. The smaller eigenvalue $\lambda_< \approx 1/2$ is a value similar to that of edge X-cycles of Wendelstein 7-X standard configuration as shown in Fig. 4. (**b**) Cartoon showing how the shift of a fixed point (for a map) is related to its starting and ending points shifts under perturbation, with a high-order version provided in Fig. 6 (Appendix A)

their corresponding trajectories are, respectively, denoted as $\boldsymbol{X}(\boldsymbol{x}_0, t)$ and $\boldsymbol{X}_{\text{pol}}(\boldsymbol{x}_{0,\text{pol}}, \phi_\text{s}, \phi_\text{e})$, $\boldsymbol{x}_0$ and $\boldsymbol{x}_{0,\text{pol}}$ are initial conditions, $\boldsymbol{B}_{\text{pol}}$ and B_ϕ are poloidal and toroidal components of the field in standard cylindrical coordinates, ϕ the azimuthal angle, ϕ_s and ϕ_e the starting and ending angles. "Toroidal" and "poloidal" are defined in the most natural way with the standard cylindrical basis:

$$\boldsymbol{B} = \underbrace{B_R\hat{\boldsymbol{e}}_R + B_Z\hat{\boldsymbol{e}}_Z}_{=:\boldsymbol{B}_{\text{pol}}} + B_\phi\hat{\boldsymbol{e}}_\phi$$

Any more complex definitions of tor- and poloidal decomposition based on various choices of flux coordinate systems are not encouraged because the flux coordinates already imply the absence of chaos, which will limit the theory to a narrower application range in which chaos is excluded. In flux coordinates, one can not explain the spiral ribbon-like footprint pattern[1] on the divertor target plates because the divertor region is outside $r = 1$ in flux coordinates.

The theory developed in this paper can be applied to general N-D systems yet is inspired by chaotic-field-related research within the MCF community, so the deduction and results are presented together with important equations numbered with suffixes a and b, respectively, to facilitate readers' choosing which form to utilize. The equations with suffix a apply to N-D systems, while the equations with suffix b directly apply to MCF, which is the main motivation to develop FPT. Notably, it is found during derivation that the vanishing divergence is not a necessary condition to keep equations concise. Hence, the theory harvests a broad application range, evolving into a general FPT that could benefit other domains than MCF.

Differentiated in the initial conditions by chain rule, Eqs.(1a),(1b) become the progression formulae of $\mathcal{D}\boldsymbol{X}$ and $\mathcal{D}\boldsymbol{X}_{\text{pol}}$ (a well-known formula in the ODE community),

$$\frac{\partial}{\partial t}\mathcal{D}\boldsymbol{X} = \nabla\boldsymbol{B}\cdot\mathcal{D}\boldsymbol{X} \tag{2a}$$

[1]Numerical results of the ribbon-like spiral footprint pattern can be found in: Figs. 2, 7, 8, 10 of [5], Fig. 11 of [6], and Fig. 2a, b of [7]. Experimental observation of strike line splitting can be found in Fig. 4 of [4], and it is reasonably consistent with the footprint pattern as shown in Fig. 5 of [4].

$$= \begin{bmatrix} \frac{\partial B_1}{\partial x_1} & \frac{\partial B_1}{\partial x_2} & \cdots & \frac{\partial B_1}{\partial x_N} \\ \vdots & & \ddots & \vdots \\ \frac{\partial B_N}{\partial x_1} & \frac{\partial B_N}{\partial x_2} & \cdots & \frac{\partial B_N}{\partial x_N} \end{bmatrix} \cdot \begin{bmatrix} \frac{\partial X_1}{\partial x_{0,1}} & \frac{\partial X_1}{\partial x_{0,2}} & \cdots & \frac{\partial X_1}{\partial x_{0,N}} \\ \vdots & & \ddots & \vdots \\ \frac{\partial X_N}{\partial x_{0,1}} & \frac{\partial X_N}{\partial x_{0,2}} & \cdots & \frac{\partial X_N}{\partial x_{0,N}} \end{bmatrix}$$

$$\underbrace{\frac{\partial}{\partial \phi_e}}_{\substack{\text{only ending angle } \phi_e \text{ changes,} \\ \text{starting angle } \phi_s \text{ is kept constant}}} \mathcal{D}\boldsymbol{X}_{\text{pol}} = \underbrace{\frac{\partial (R\boldsymbol{B}_{\text{pol}}/B_\phi)}{\partial (R, Z)}}_{\text{abbr. as } \mathbf{A}=\mathbf{A}(R,Z,\phi)} \cdot \mathcal{D}\boldsymbol{X}_{\text{pol}} \tag{2b}$$

where $\mathcal{D}$ means the partial derivative *w.r.t.* $\boldsymbol{x}_0$ or $\boldsymbol{x}_{0,\text{pol}}$. Note that $\mathbf{A} = \mathbf{A}(R, Z, \phi)$ is a function of spatial coordinates directly, $\boldsymbol{X}_{\text{pol}}(\boldsymbol{x}_{0,\text{pol}}, \phi_s, \phi_e)$ is a function of the initial point (not *in-situ*). To emphasize the difference, two derivative operators $\partial/\partial(R, Z)$ and $\mathcal{D}$ are used.

The term *X-cycle* is a figurative alias of *hyperbolic cycle* (see Fig. 1a). A cycle is *hyperbolic* if

$$|\lambda_i| \neq 1 \text{ for all eigenvalues of } \mathcal{D}\mathcal{P}^m,$$
$$\text{or equiv. } |\lambda_i| \neq 1 \text{ for all eigenvalues of } \mathcal{D}\boldsymbol{X}_T \text{ except}$$

the one corresponding to the eigenvector $\boldsymbol{v}_i = \hat{\boldsymbol{b}}$, where $\hat{\boldsymbol{b}}$ is the local field normalized. An O-cycle can be similarly defined in 3D continuous-time systems with both $\mathcal{D}\mathcal{P}^m$ eigenvalues $\lambda_i \in \mathbb{S} \subset \mathbb{C}$ but $\neq \pm 1$. $\mathcal{P}$ denotes the Poincaré map. In this paper, for a 3D toroidal vector field, the Poincaré section is simply chosen to be an R-Z cross-section, while m is the toroidal turn number of the cycle, to align with the MCF convention that m denotes the poloidal mode number, which is also the toroidal turn number of a cycle on a rational flux surface. For a general N-D system, $\mathcal{P}^m$ can be defined as a whole with no individual meaning of m to express the returning map for quasi-periodic cases.

The evolutions of $\mathcal{D}\boldsymbol{X}_T$ and $\mathcal{D}\mathcal{P}^m$ along a cycle have been revealed by two formulae given in [31] as shown below:

$$\frac{\mathrm{d}}{\mathrm{d}t}\mathcal{D}\boldsymbol{X}_T = [\nabla \boldsymbol{B}, \mathcal{D}\boldsymbol{X}_T] \tag{3a}$$

$$\frac{\mathrm{d}}{\mathrm{d}\phi}\mathcal{D}\mathcal{P}^m = \left[\frac{\partial (R\boldsymbol{B}_{\text{pol}}/B_\phi)}{\partial (R, Z)}, \mathcal{D}\mathcal{P}^m\right] = [\mathbf{A}, \mathcal{D}\mathcal{P}^m]. \tag{3b}$$

where $\mathcal{D}\boldsymbol{X}_T$ is short for the full-period Jacobian of the cycle in N-D systems, that is $\mathcal{D}\boldsymbol{X}(\boldsymbol{x}_0, T)|_{\boldsymbol{x}_0 = \boldsymbol{X}(\boldsymbol{x}_{\text{fix}}, t)}$, $\boldsymbol{x}_{\text{fix}}$ is a fixed point on the cycle, and $\mathcal{D}\mathcal{P}^m$ has been introduced before as a counterpart of the former one in cylindrical coordinates. The square bracket denotes the commutator, $[\mathbf{A}, \mathbf{B}] := \mathbf{A} \cdot \mathbf{B} - \mathbf{B} \cdot \mathbf{A}$.

The formulae above are presented in a general form, enabling readers to substitute the system $\boldsymbol{B}$ with one relevant to their context. For instance, consider the non-relativistic equation of motion for a charged particle:

$$\dot{\boldsymbol{X}} = \begin{bmatrix} \dot{\boldsymbol{x}} \\ \dot{\boldsymbol{v}} \end{bmatrix} = \begin{bmatrix} \boldsymbol{v} \\ \frac{q}{m}(\boldsymbol{E} + \boldsymbol{v} \times \boldsymbol{B}) \end{bmatrix},$$

The $\nabla \boldsymbol{B}$ appearing in the progression (2a) and evolution (3a) formulae can be substituted and evaluated as

$$\begin{bmatrix} \partial \boldsymbol{v}/\partial \boldsymbol{x} & \partial \boldsymbol{v}/\partial \boldsymbol{v} \\ \frac{q}{m}(\nabla \boldsymbol{E} + \boldsymbol{v} \times \nabla \boldsymbol{B}) & \frac{q}{m}\partial(\boldsymbol{v} \times \boldsymbol{B})/\partial \boldsymbol{v} \end{bmatrix} = \begin{bmatrix} \mathbf{0}_{3\times 3} & \mathbf{I}_{3\times 3} \\ \frac{q}{m}(\nabla \boldsymbol{E} + \boldsymbol{v} \times \nabla \boldsymbol{B}) & -\frac{q}{m}[\boldsymbol{B}]_\times \end{bmatrix}$$

where $\mathbf{0}_{3\times 3}$ is simply the zero square matrix, $\mathbf{I}_{3\times 3}$ the identity matrix, and $[\boldsymbol{B}]_\times$ the skew-symmetric matrix conventionally representing the cross product with $\boldsymbol{B}$.

$$[\boldsymbol{B}]_\times := \begin{bmatrix} 0 & -B_z & B_y \\ B_z & 0 & -B_x \\ -B_y & B_x & 0 \end{bmatrix}.$$

These formulae compute the sensitivity matrix $\mathcal{D}_{(\boldsymbol{x}_0, \boldsymbol{v}_0)}\boldsymbol{X}(\ (\boldsymbol{x}_0, \boldsymbol{v}_0), t)$, quantifying how variations in initial conditions influence the trajectory within the 6D phase space. The charged particle motion model serves as a pedagogical example. In magnetically confined fusion (MCF), the magnetic field-line tracing system is of paramount importance, as the magnetic topology primarily governs radial transport.

2.1 Functional derivative notations

Partial and total functional derivatives are denoted, respectively, by

$$\delta/\delta\mathcal{B} \quad \text{and} \quad \mathrm{d}/\mathrm{d}\mathcal{B},$$

but they are inconvenient to use due to their infinite-dimensional nature. Hence, they are often accompanied by a given perturbation $\Delta\mathcal{B}$ to be directional derivatives

$$\Delta\mathcal{B}\cdot\delta/\delta\mathcal{B} \quad \text{and} \quad \Delta\mathcal{B}\cdot\mathrm{d}/\mathrm{d}\mathcal{B}.$$

In this and upcoming FPT papers, when $\boldsymbol{B}$ is written in calligraphic font $\mathcal{B}$, it means $\mathcal{B}$ is not to be evaluated at a specific point but considered as a standalone object. Let $\boldsymbol{X}[\mathcal{B}]$ be a function dependent on the system. An alternative notation of directional partial derivative equivalent to $\prod_k(\Delta\mathcal{B}_k\cdot\delta/\delta\mathcal{B})\boldsymbol{X}$ is

$$\delta^k\boldsymbol{X}[\mathcal{B};\Delta\mathcal{B}_1,\ldots,\Delta\mathcal{B}_k] \quad \text{(a common notation, e.g. in [32])},$$

of which the argument list can be omitted for brevity if the context is clear especially when all $\Delta\mathcal{B}_k$ are the same, simply written as $\delta^k\boldsymbol{X}$. A perturbation $\Delta\mathcal{B}$ can be decomposed into different orders as follows,

$$\mathcal{B}+\Delta\mathcal{B}=\mathcal{B}+\delta\mathcal{B}+\frac{1}{2!}\delta^2\mathcal{B}+\frac{1}{3!}\delta^3\mathcal{B}+\cdots.$$

To extract the k-th order term, evaluate the directional functional derivative $\delta^k\boldsymbol{B}[\mathcal{B};\Delta\mathcal{B},\ldots,\Delta\mathcal{B}](\boldsymbol{x})$ at every point in the domain. With function arguments removed, the result can be simply denoted as $\delta^k\boldsymbol{B}(\boldsymbol{x})$. Collecting these variations across the domain allows one to construct the k-th order component of the perturbation, denoted by $\delta^k\mathcal{B}$. Conversely, one can also define a perturbation $\Delta\mathcal{B}$ by specifying a sequence of $\delta^k\mathcal{B}$.

For instance, $\boldsymbol{J}\times\boldsymbol{B}=\nabla p$ is the force balance equation in static, single-fluid, ideal magnetohydrodynamics. Upon functional derivatives,

$$\begin{aligned}\boldsymbol{J}\times\boldsymbol{B}=&\nabla p \quad \text{becomes}\\ \delta\boldsymbol{J}\times\boldsymbol{B}+\boldsymbol{J}\times\delta\boldsymbol{B}=&\delta\nabla p\\ \delta^2\boldsymbol{J}\times\boldsymbol{B}+2\delta\boldsymbol{J}\times\delta\boldsymbol{B}+\boldsymbol{J}\times\delta^2\boldsymbol{B}=&\delta^2\nabla p\\ &\vdots\end{aligned}$$

Then one can write

$$(\boldsymbol{J}+\Delta\boldsymbol{J})\times(\boldsymbol{B}+\Delta\boldsymbol{B})=\nabla p+\Delta\nabla p,$$

with $\Delta\boldsymbol{J}$, $\Delta\boldsymbol{B}$ and $\Delta\nabla p$ defined by their corresponding series expansions.

3 Deduction and demonstration

With the whole system $\mathcal{B}$ considered as an argument of a trajectory $\boldsymbol{X}$ in an N-D system, Eq. (2a) becomes

$$\frac{\partial}{\partial t}\boldsymbol{X}[\mathcal{B}](\boldsymbol{x}_0,t)=\boldsymbol{B}(\boldsymbol{X})=\boldsymbol{B}[\mathcal{B}](\boldsymbol{X}[\mathcal{B}](\boldsymbol{x}_0,t)). \tag{4}$$

Imposed directional functional derivatives on both sides, the above equation converts to the first-order progression formula of trajectory shift under perturbation,

$$\frac{\partial}{\partial t}\delta\boldsymbol{X}[\mathcal{B};\Delta\mathcal{B}](\boldsymbol{x}_0,t)=\delta\boldsymbol{B}[\mathcal{B};\Delta\mathcal{B}](\boldsymbol{X}[\mathcal{B}](\boldsymbol{x}_0,t))+\delta\boldsymbol{X}[\mathcal{B};\Delta\mathcal{B}](\boldsymbol{x}_0,t)\cdot\nabla\boldsymbol{B} \tag{5}$$

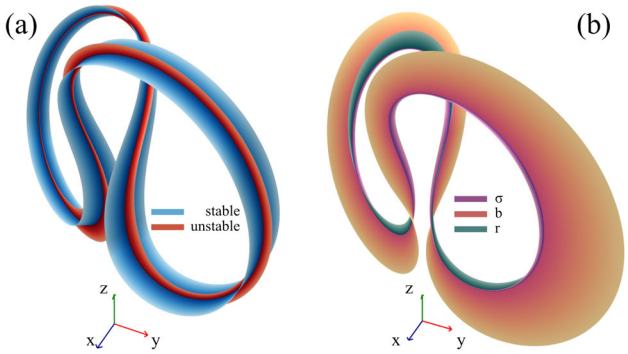

Fig. 2 A typical cycle of Lorenz attractor. (**a**) Sprouts of stable and unstable manifolds indicated by $\mathcal{D}\boldsymbol{X}_T$ eigenvectors (except the one $\boldsymbol{v}_i = \hat{\boldsymbol{b}}$). (**b**) The first variation of the cycle position perpendicular shift $\delta_\perp \boldsymbol{x}_{\text{cyc}}[\mathcal{B}; \Delta\mathcal{B}]$, $\Delta\mathcal{B} \in [\mathcal{B}_\sigma, \mathcal{B}_b, \mathcal{B}_r]$

With arguments omitted, the above formula (5) becomes

$$\frac{\partial}{\partial t}\delta\boldsymbol{X} = \delta\boldsymbol{B} + (\delta\boldsymbol{X}\cdot\nabla)\boldsymbol{B}, \tag{6a}$$

along with its counterpart in cylindrical coordinates

$$\frac{\partial}{\partial \phi_{\text{e}}}\delta\boldsymbol{X}_{\text{pol}} = \delta\left(\frac{R\boldsymbol{B}_{\text{pol}}}{B_\phi}\right) + \left(\delta\boldsymbol{X}_{\text{pol}}\cdot\frac{\partial}{\partial(R,\,Z)}\right)\frac{R\boldsymbol{B}_{\text{pol}}}{B_\phi}. \tag{6b}$$

Similarly, for the second variation,

$$\frac{\partial}{\partial t}\delta^2\boldsymbol{X} = \delta^2\boldsymbol{B} + 2(\delta\boldsymbol{X}\cdot\nabla)\delta\boldsymbol{B} + \delta\boldsymbol{X}\delta\boldsymbol{X} : \nabla^2\boldsymbol{B} + \delta^2\boldsymbol{X}\cdot\nabla\boldsymbol{B}, \tag{7}$$

where the colon is defined as $\boldsymbol{ab} : \boldsymbol{cd} = (\boldsymbol{a}\cdot\boldsymbol{c})(\boldsymbol{b}\cdot\boldsymbol{d})$, and more dots arranged vertically simply mean more times of dot product such as $abc \vdots def = (a\cdot d)(b\cdot e)(c\cdot f)$.

The deduction can be continued to higher orders, e.g., the third variation progresses as below,

$$\begin{aligned}\frac{\partial}{\partial t}\delta^3\mathbf{X} = {}& \delta^3\mathbf{B} + 3(\delta\mathbf{X}\cdot\nabla)\delta^2\mathbf{B} \\ & + 3(\delta^2\mathbf{X}\cdot\nabla)\delta\mathbf{B} + 3(\delta\mathbf{X}\delta\mathbf{X} : \nabla^2)\delta\mathbf{B} \\ & + 3\delta\mathbf{X}\delta^2\mathbf{X} : \nabla^2\mathbf{B} + \delta\mathbf{X}\delta\mathbf{X}\delta\mathbf{X} \vdots \nabla^3\mathbf{B} + \delta^3\mathbf{X}\cdot\nabla\mathbf{B}.\end{aligned} \tag{8}$$

For arbitrary finite order, please check the formula (A11) in Appendix A.

The shift of a trajectory under system-wide perturbation can be approximated by the following Taylor expansion based on these variations,

$$\boldsymbol{X}[\mathcal{B}+\Delta\mathcal{B}](\boldsymbol{x}_0,\,t) = \boldsymbol{X}[\mathcal{B}](\boldsymbol{x}_0,\,t) + \delta\boldsymbol{X} + \delta^2\boldsymbol{X}/2! + \cdots + \delta^k\boldsymbol{X}/k! + \mathcal{O}(\|\Delta\mathcal{B}\|^{k+1}). \tag{9}$$

3.1 Lorenz attractor as an educational demonstration

The Lorenz attractor (Figs. 2 and 3) is employed here as a pedagogical example to illustrate the power-law scaling of error. Parameters are set as $\sigma = 10$, $r = 28$, and $b = 8/3$, a standard and widely used configuration. The simplest cycle listed in Table 1 of [33] with a period of $T = 1.5586522107162$ and initial condition

$$\boldsymbol{x}_0 = [-13.763610682134,\quad -19.578751942452,\quad 27]$$

is chosen to illustrate the sprouts of its stable and unstable manifolds as shown in Fig. 2a. The shift tendencies of this cycle in Lorenz attractor system,

$$\boldsymbol{B} = \begin{bmatrix}\sigma(-x+y)\\ -xz+rx-y\\ xy-bz\end{bmatrix},$$

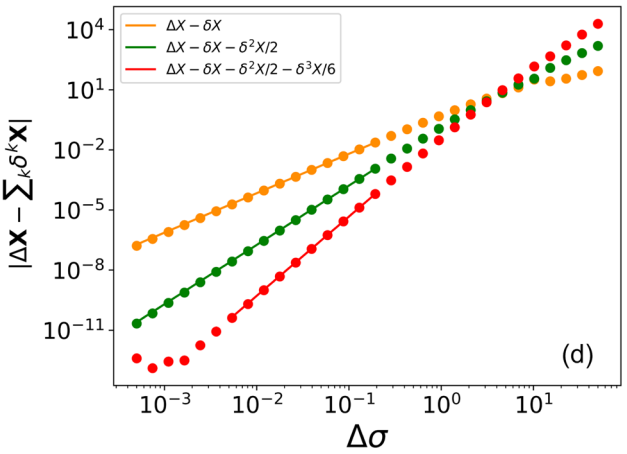

Fig. 3 The approximation errors against $\Delta\sigma$ for a trajectory initiating from the same point $\boldsymbol{x}_0$ as that of the chosen cycle. The errors are evaluated at $t = 1.0$

perturbed by varying σ, r and b, i.e.,

$$\Delta_\sigma \boldsymbol{B} = \Delta\sigma \begin{bmatrix} -x+y \\ 0 \\ 0 \end{bmatrix}, \quad \Delta_r \boldsymbol{B} = \Delta r \begin{bmatrix} 0 \\ x \\ 0 \end{bmatrix}, \qquad \Delta_b \boldsymbol{B} = \Delta b \begin{bmatrix} 0 \\ 0 \\ -z \end{bmatrix}$$

are shown in Fig. 2b.

Then one shall expect the approximation error $|\Delta \boldsymbol{X} - \sum_k \delta^k \boldsymbol{X}|$ to be an order of $\mathcal{O}(\Delta\sigma^{k+1})$ if only σ is perturbed, where $\Delta \boldsymbol{X} := \boldsymbol{X}[\mathcal{B} + \Delta\mathcal{B}] - \boldsymbol{X}[\mathcal{B}]$. In other words,

$$\ln(\text{err}) \propto k_{\text{err}} \ln \Delta\sigma, \quad k_{\text{err}} \geq k+1, \tag{10}$$

which is verified in Fig. 3 by fitting the scatters. The fitted slopes for the first three-order approximations, as shown by straight lines in Fig. 3, equal 1.96772, 2.96082, 3.95880, respectively. The fitted slopes coincide well with $k+1$ as expected.

To migrate Eqs. (4–8) from continuous flows to discrete maps, e.g., a general map $\mathcal{P} : \mathbb{R}^N \to \mathbb{R}^N$, one simply needs to replace $\partial \boldsymbol{X}/\partial t$ on the left hand side (LHS) with $\mathcal{P}^{k+1}(\boldsymbol{x})$, and $\boldsymbol{X}$ on the right-hand side (RHS) with $\mathcal{P}^k(\boldsymbol{x})$. For example, Eq. (4) becomes

$$\mathcal{P}^{k+1}[\mathcal{P}](\boldsymbol{x}) = \mathcal{P}[\mathcal{P}](\mathcal{P}^k[\mathcal{P}](\boldsymbol{x})), \tag{11}$$

Equations (4–9) do not need to make substantial change if the system is non-autonomous, i.e., the time is an explicit variable of the field $\boldsymbol{B} = \boldsymbol{B}(t, \boldsymbol{x})$. Only when one is concerned about how to define a *periodic* trajectory does the difference between autonomous and non-autonomous manifests. For example, a boomerang thrower on a moving train would argue that the trajectory is periodic only if the boomerang returns to his position. To maintain simplicity, this paper considers periodic orbits exclusively in autonomous systems, e.g., a time slice of a magnetic field, ensuring that the concept of "*periodic*" remains straightforward and uncontested.

3.2 The shift of a cycle

Thereafter, one can calculate the shift of a cycle based on the first variation $\delta\mathcal{P}^m$ with the aid of $\mathcal{DP}^m$, as explained in Fig. 1b. Note that a periodic orbit and a cycle are defined to be those that have the initial points tied to the ending points. The idea to calculate the shift is $\boldsymbol{x}_{\text{cyc}}$ must have such a shift $\Delta\boldsymbol{x}_{\text{cyc}}$ that the ending point $\mathcal{P}(\boldsymbol{x}_{\text{cyc}})$ after perturbation keeps matching the starting point, i.e.,

$$\Delta\boldsymbol{x}_{\text{cyc}} = \Delta\mathcal{P}^m(\boldsymbol{x}_{\text{cyc}}) + \mathcal{DP}^m(\boldsymbol{x}_{\text{cyc}}) \cdot \Delta\boldsymbol{x}_{\text{cyc}} + \cdots, \tag{12}$$

$$\begin{aligned} \Delta\boldsymbol{x}_{\text{cyc}} &= [\mathcal{DP}^m(\boldsymbol{x}_{\text{cyc}}) - \mathbf{I}]^{-1} \cdot [-\Delta\mathcal{P}^m(\boldsymbol{x}_{\text{cyc}})] \\ &= [\mathcal{DP}^m(\boldsymbol{x}_{\text{cyc}}) - \mathbf{I}]^{-1} \cdot \\ &\quad \Big(- \delta\mathcal{P}^m[\mathcal{B}; \Delta\mathcal{B}](\boldsymbol{x}_{\text{cyc}}) + \mathcal{O}(\|\Delta\mathcal{B}\|^2) \Big) + \cdots, \end{aligned} \tag{13}$$

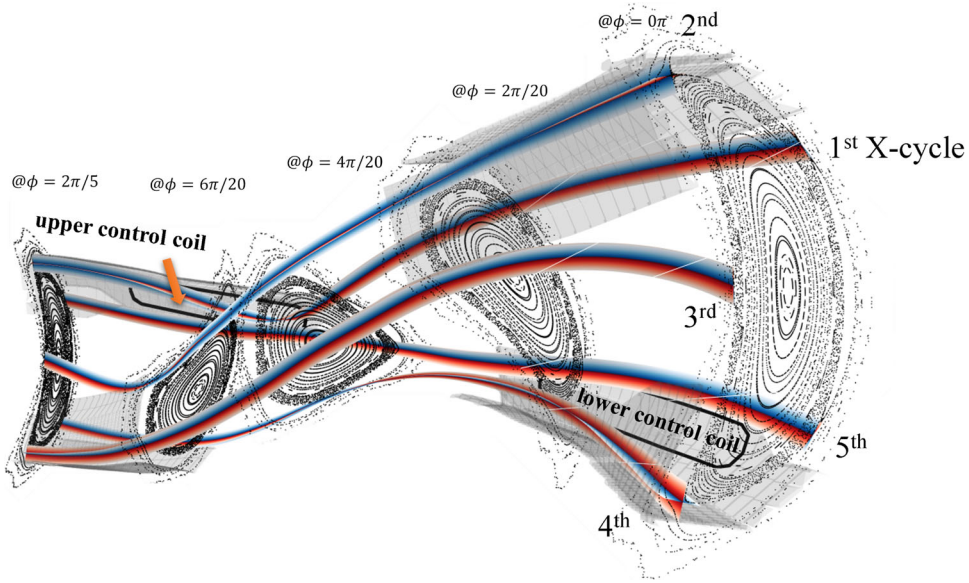

Fig. 4 Five typical Poincaré plots for Wendelstein 7-X standard configuration. Red and blue ribbons *resp.* indicate the directions of $\mathcal{DP}^1$ $(m = 1)$ unstable and stable eigenvectors corresponding to $\lambda_i = 1.94965374$ and 0.51291252

$\delta\mathcal{P}^m$ on RHS contributes the first-order variation; hence,

$$\delta \boldsymbol{x}_{\text{cyc}} = -[\mathcal{DP}^m - \mathbf{I}]^{-1} \cdot \delta\mathcal{P}^m, \tag{14}$$

which applies to periodic orbits and cycles whose full-period Jacobians $\mathcal{DP}^m$ do not have eigenvalues equal to one. For those on center manifolds, this condition is broken, requiring a different analysis. Deduction for higher order $\delta^k \boldsymbol{x}_{\text{cyc}}$ is put in Appendix A.

To apply Eq. (14) to an N-D flow, one needs to define a local $(N-1)$-D Poincaré plane for every point on the concerned cycle to define Poincaré map. A natural choice is the local plane perpendicular to the cycle. To avoid constructing one more frame of coordinates on the plane, a suggested way is to utilize the relationship between $\mathcal{D}\boldsymbol{X}_T$ and this local Poincaré map Jacobian $\mathcal{DP}^m$. $\mathcal{DP}^m$ has the same eigenvalues λ_i as $\mathcal{D}\boldsymbol{X}_T$ but with eigenvectors projected to the Poincaré plane $\boldsymbol{v}_{i\perp} = \boldsymbol{v}_i - \hat{\boldsymbol{b}}\hat{\boldsymbol{b}}^T \cdot \boldsymbol{v}_i$. Decompose $\Delta\boldsymbol{x}_{\text{cyc}}$ to be the sum of eigenvectors as $\Delta\boldsymbol{x}_{\text{cyc}} \approx \delta_\perp \boldsymbol{x}_{\text{cyc}} = \sum c_i \boldsymbol{v}_{i\perp}$. Then one can replace $\mathcal{DP}^m(\boldsymbol{x}_{\text{cyc}}) \cdot \Delta\boldsymbol{x}_{\text{cyc}}$ in Eq. (12) with $\sum c_i \lambda_i \boldsymbol{v}_{i\perp}$ and $\Delta\mathcal{P}^m(\boldsymbol{x}_{\text{cyc}})$ with its first variation $\delta_\perp \boldsymbol{X}_T := \delta\boldsymbol{X}_T - \hat{\boldsymbol{b}}\hat{\boldsymbol{b}}^T \cdot \delta\boldsymbol{X}_T$. Then one can solve for the coefficients c_i to determine $\delta_\perp \boldsymbol{x}_{\text{cyc}}$.

The other way to solve for the cycle shift is to reuse the definition of "*periodic*": the starting and ending points are tied, but this time one should take into account projecting $\delta\boldsymbol{X}_T$ and $\mathcal{D}\boldsymbol{X}_T \cdot \delta_\perp \boldsymbol{x}_{\text{cyc}}$ to the perpendicular Poincaré plane as below,

$$\delta_\perp \boldsymbol{x}_{\text{cyc}} = (\mathbf{I} - \hat{\boldsymbol{b}}\hat{\boldsymbol{b}}^T) \cdot \delta\boldsymbol{X}_T + (\mathbf{I} - \hat{\boldsymbol{b}}\hat{\boldsymbol{b}}^T) \cdot \mathcal{D}\boldsymbol{X}_T \cdot \delta_\perp \boldsymbol{x}_{\text{cyc}}, \tag{15}$$

of which the LHS is the starting point shift, while the RHS is the ending point shift that consists of two terms: the first one is contributed by the perturbation and the second one is propagated from the starting point shift via $\mathcal{D}\boldsymbol{X}_T$. Reorganize Eq (15) to be

$$\delta_\perp \boldsymbol{x}_{\text{cyc}} = \left[\mathbf{I} - (\mathbf{I} - \hat{\boldsymbol{b}}\hat{\boldsymbol{b}}^T) \cdot \mathcal{D}\boldsymbol{X}_T\right]^{-1} \cdot (\mathbf{I} - \hat{\boldsymbol{b}}\hat{\boldsymbol{b}}^T) \cdot \delta\boldsymbol{X}_T. \tag{16}$$

3.3 Evolution of cycle shift along a cycle

To avoid repetitive calculation of $\delta\boldsymbol{X}_T$ and $\delta\mathcal{P}^m$ for every point on a cycle, their evolutions along the cycle are concluded as the following formulae,

$$\frac{\mathrm{d}}{\mathrm{d}t}\delta\boldsymbol{X}_T = \nabla\boldsymbol{B} \cdot \delta\boldsymbol{X}_T - (\mathcal{D}\boldsymbol{X}_T - \mathbf{I}) \cdot \delta\boldsymbol{B}, \tag{17a}$$

$$\frac{\mathrm{d}}{\mathrm{d}\phi}\delta\mathcal{P}^m = \frac{\partial(R\boldsymbol{B}_{\text{pol}}/B_\phi)}{\partial(R,\, Z)} \cdot \delta\mathcal{P}^m - (\mathcal{DP}^m - \mathbf{I}) \cdot \delta\frac{R\boldsymbol{B}_{\text{pol}}}{B_\phi}, \tag{17b}$$

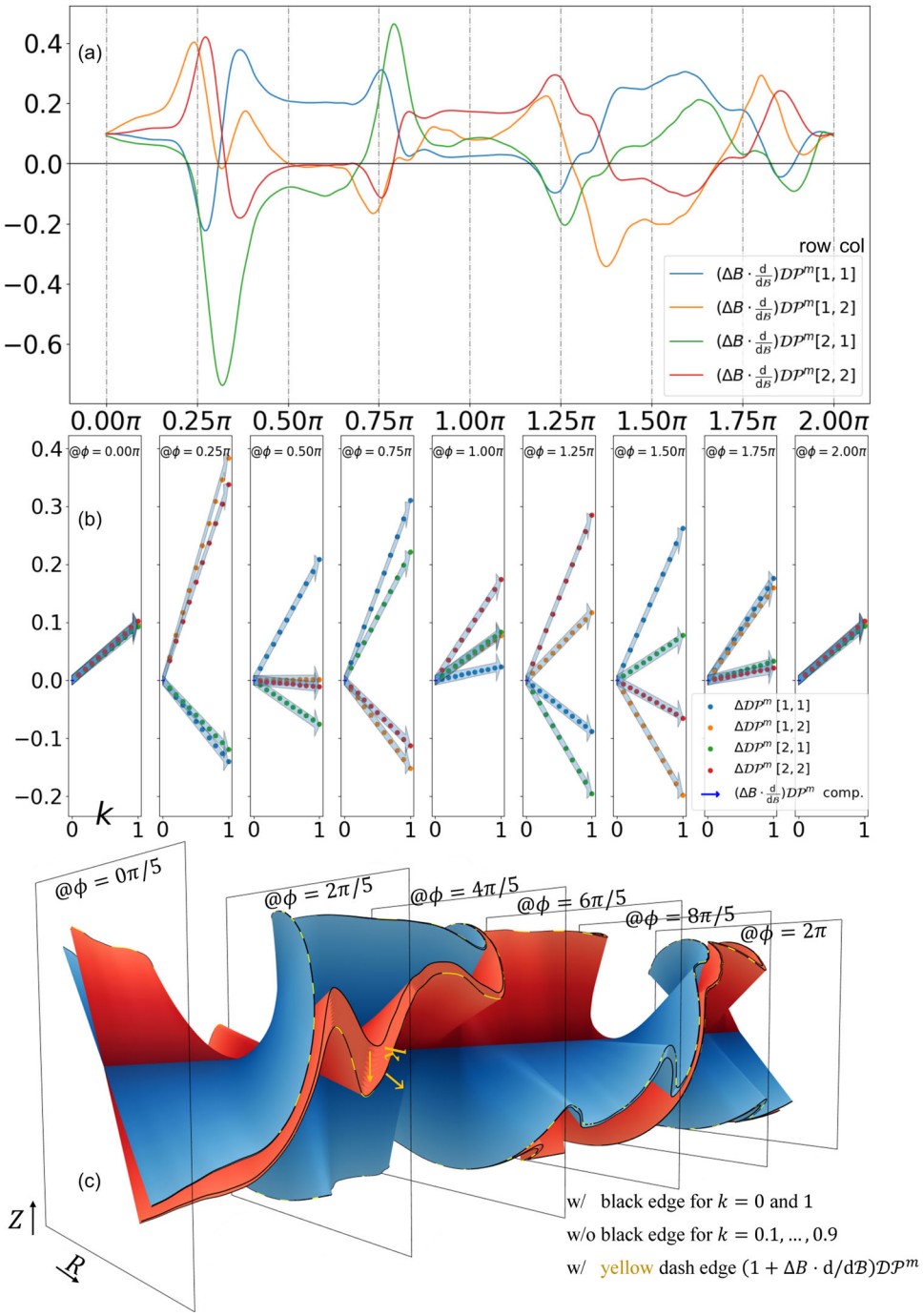

Fig. 5 The change of $\mathcal{DP}^m$ of the first X-cycle at the edge $\iota = n/m = 5/5$ island chain of Wendelstein 7-X standard configuration under the perturbation of upper control coils (each 1kA). $(\Delta\mathcal{B} \cdot \mathrm{d}/\mathrm{d}\mathcal{B})\mathcal{DP}^m$ components are shown as curves in (**a**) and as transparent blue arrows in (**b**). Scatter points in (**b**) show the reference values for the changes of $\mathcal{DP}^m$ components computed for each k in a brute-force way. (**c**) $\mathcal{DP}^m$ eigenvectors against ϕ

where $\delta(R\boldsymbol{B}_{\mathrm{pol}}/B_\phi)$ is short for $(\Delta\mathcal{B}\cdot\delta/\delta\mathcal{B})(R\boldsymbol{B}_{\mathrm{pol}}/B_\phi)$, equal to $\left(\dfrac{R\,\delta\boldsymbol{B}_{\mathrm{pol}}}{B_\phi} - \dfrac{R\boldsymbol{B}_{\mathrm{pol}}}{B_\phi^2}\cdot\delta B_\phi\right)$ by the product rule of differentiation.

Similarly, the calculation of the first-order cycle shift $\delta\boldsymbol{x}_{\mathrm{cyc}}$ given by Eq. (14) is just for one cross-section. To acquire $\delta\boldsymbol{x}_{\mathrm{cyc}}$ for all cross-sections, the formulae governing its evolution along a cycle are concluded as below

$$\frac{\mathrm{d}}{\mathrm{d}t}\delta_\perp\boldsymbol{x}_{\mathrm{cyc}} \not\equiv \nabla\boldsymbol{B}\cdot\delta_\perp\boldsymbol{x}_{\mathrm{cyc}} + \delta\boldsymbol{B}, \tag{18a'}$$

$$\frac{\mathrm{d}}{\mathrm{d}t}\delta\boldsymbol{x}_{\mathrm{cyc}} = \nabla\boldsymbol{B}\cdot\delta\boldsymbol{x}_{\mathrm{cyc}} + \delta\boldsymbol{B}, \tag{18a}$$

$$\frac{\mathrm{d}}{\mathrm{d}\phi}\delta\boldsymbol{x}_{\mathrm{cyc}} = \frac{\partial(R\boldsymbol{B}_{\mathrm{pol}}/B_\phi)}{\partial(R,\,Z)}\cdot\delta\boldsymbol{x}_{\mathrm{cyc}} + \delta\frac{R\boldsymbol{B}_{\mathrm{pol}}}{B_\phi}. \tag{18b}$$

A concise expression like Eq. (18a′) for the *perpendicular* shift in an N-D flow as a counterpart of the other two equations has not been found. That is why Eq. (18a′) with a prime over 18a does not hold. Instead, Eq. (18a) holds for the full variation $\delta\boldsymbol{x}_{\mathrm{cyc}}$ including both the shift *perpendicular* to and that *parallel* to the local field, which reuses Eq. (6a) but now plays a role of an evolution formula (18a) instead of a progression one by setting the initial condition $\delta\boldsymbol{x}_{\mathrm{cyc}}(t=0)$ to equal the initial, perpendicular or not, shift vector instead of a zero vector. The parallel shift component can take any value because a point moving in this direction still remains on the cycle.

What the authors deduced for the perpendicular shift in N-D case, that is the true right-hand side of Eq. (18a′), is too verbose to be a formula, of which the main complexity comes from the fact that $\hat{\boldsymbol{b}}$ changes along the cycle so the result involves $\boldsymbol{B}\cdot\nabla\hat{\boldsymbol{b}}$ and becomes difficult to reduce, which is elaborated in great details in Appendix B along with a proof of the formula (18b).

3.4 The change of full-period Jacobian $\mathcal{DP}^m$

Hereafter, the full-period Jacobian on a cycle and its change under perturbation will be examined. As a first step, with the whole system $\mathcal{B}$ considered as an argument, the Jacobian progression formula $\partial_{\phi_\mathrm{e}}\mathcal{D}\boldsymbol{X}_{\mathrm{pol}}(\boldsymbol{x}_{0,\,\mathrm{pol}},\,\phi_\mathrm{s},\,\phi_\mathrm{e}) = \mathbf{A}\bullet\mathcal{D}\boldsymbol{X}_{\mathrm{pol}}$ (2b) is complicated into

$$\begin{aligned}&\frac{\partial}{\partial\phi_\mathrm{e}}\mathcal{D}\boldsymbol{X}_{\mathrm{pol}}[\mathcal{B}](\boldsymbol{x}_{\mathrm{cyc}}[\mathcal{B}](\phi_\mathrm{s}),\,\phi_\mathrm{s},\,\phi_\mathrm{e})\\ &\quad= \mathbf{A}[\mathcal{B}](\boldsymbol{x}_{\mathrm{cyc}}[\mathcal{B}](\phi_\mathrm{e}),\,\phi_\mathrm{e})\bullet\mathcal{D}\boldsymbol{X}_{\mathrm{pol}}[\mathcal{B}](\boldsymbol{x}_{\mathrm{cyc}}[\mathcal{B}](\phi_\mathrm{s}),\,\phi_\mathrm{s},\,\phi_\mathrm{e}),\end{aligned} \tag{19}$$

of which an integration in ϕ_e after imposed $\Delta\mathcal{B}\cdot\frac{\mathrm{d}}{\mathrm{d}\mathcal{B}}$ gives $(\Delta\mathcal{B}\cdot\frac{\mathrm{d}}{\mathrm{d}\mathcal{B}})\mathcal{D}\boldsymbol{X}_{\mathrm{pol}}$ on LHS. Note that this is a total derivative considering the influence from the $\boldsymbol{x}_{\mathrm{cyc}}$ shift. The $\mathcal{DP}^m$ evolution formula $\frac{\mathrm{d}}{\mathrm{d}\phi}\mathcal{DP}^m = \left[\mathbf{A},\,\mathcal{DP}^m\right]$ (3b) can be similarly processed, which yields $(\Delta\mathcal{B}\cdot\frac{\mathrm{d}}{\mathrm{d}\mathcal{B}})\mathcal{DP}^m$ on all sections. The relevant deduction is put in Appendix C.

As a practical demonstration, the $\mathcal{DP}^m$ of X-cycles at the edge island chain in the standard configuration of Wendelstein 7-X on all ϕ-sections have been calculated and shown in Fig. 4 by the eigenvectors. Let the vacuum field of the upper control coils (upCC) be the perturbation, i.e., $\mathcal{B}+\Delta\mathcal{B} = \mathcal{B}_{\mathrm{std}} + k\delta\mathcal{B}_{\mathrm{upCC}}$. The computed $(\Delta\mathcal{B}\cdot\frac{\mathrm{d}}{\mathrm{d}\mathcal{B}})\mathcal{DP}^m$ are verified by results acquired in a brute-force way (that is, simply relocate the X-cycle and recalculate $\mathcal{DP}^m$), as shown in Fig. 5c, where the eigenvectors of $\mathcal{DP}^m$ at different k are drawn as ribbons to present the change tendency vividly. The yellow dashed edges corresponding to the computed $(1+\Delta\mathcal{B}\cdot\frac{\mathrm{d}}{\mathrm{d}\mathcal{B}})\mathcal{DP}^m$ match the black edge lines corresponding to $k=1$ acquired in the brute-force way as expected.

The theory can be applied not only to fix an X-cycle at a specified position in the divertor region or push back the magnetic axis (O-cycle) against Shafranov shift, but also to maintain the eigenvalues of $\mathcal{DP}^m$ close to unity during operation. This ensures longer field-line connection lengths, which facilitates detachment, and can be employed to counteract potentially detrimental effects induced by the chaotized lobe structure [34–37] because fragile components may be strafed.

4 Discussion and conclusion

As common in tokamak detachment physics [38–40], a simple criterion for detachment, based on the principle that the total conductive power entering the scrape-off layer can be dissipated through volumetric losses, is expressed as:

$$\frac{14}{3}c_Z L_Z n_\mathrm{u}^2 l_\parallel > q_\mathrm{u},$$

which highlights the key variables influencing the process:

- c_Z (impurity fraction),
- L_Z (plasma radiation efficiency),
- n_u (upstream density),
- q_u (parallel upstream heat flux), and

- $l_\parallel$ (connection length).

While traditional approaches often focus on increasing c_Z or L_Z by introducing impurities, these methods risk core plasma contamination, posing challenges for sustained detachment. Functional Perturbation Theory (FPT), by contrast, provides a novel perspective by enabling precise control of the magnetic topology to enhance $l_\parallel$ without introducing impurities.

FPT emphasizes the significance of $\mathcal{DP}^m$, the Jacobian matrix associated with periodic magnetic field lines, e.g., the X-points of various tokamak and stellarator divertor configurations. By adjusting $\mathcal{DP}^m$, FPT directly influences the convergence or divergence rates of field lines near the divertor X-points, effectively increasing $l_\parallel$.

This increase in $l_\parallel$ not only facilitates detachment but also leads to downstream plasma accumulation, reminiscent of traffic congestion. This phenomenon raises the upstream density n_u, making detachment more feasible for MCF devices. Unlike prior efforts, which primarily focused on mechanically elongating divertor legs, this approach directly leverages magnetic topology, an aspect that has received comparatively little attention in detachment research.

By utilizing FPT, $l_\parallel$ can be extended efficiently, eliminating the need for impurity-driven strategies and their associated risks to core plasma. This framework provides a deeper understanding of the detachment process and establishes a robust foundation for improving magnetic configurations in pursuit of efficient and sustainable detachment.

Moreover, this theory has implications beyond MCF research, offering insights into the behavior and sensitivity to perturbation of complex systems in various domains. Agile and accurate prediction of orbit shifts under perturbation can guide practitioners in quickly identifying the desired perturbation to the system. While this work primarily focuses on the theoretical development of FPT, its potential for experimental applications extends well beyond MCF. To maintain relevance for a broader audience across general domains, detailed experimental validations specific to MCF are not elaborated here. Nonetheless, the geometric implications of the theory make its impact on MCF devices both evident and promising, offering a clear path for future experimental studies. A critical aspect is understanding the geometric significance of $\mathcal{DP}^m$ and the ability to compute its variation *a priori*, providing a foundational tool for predicting and controlling system responses to perturbations.

This work was supported by the National Key R&D Program of China (Grant No. 2022YFE03050003). This work has been carried out within the framework of the EUROfusion Consortium, funded by the European Union via the Euratom Research and Training Program (Grant Agreement No 101052200 -EUROfusion). Views and opinions expressed are, however, those of the author(s) only and do not necessarily reflect those of the European Union or the European Commission. Neither the European Union nor the European Commission can be held responsible for them. Additionally, the author Wenyin Wei would like to express his gratitude to the China Scholarship Council for providing financial support for his doctoral joint cultivation in Europe.

Funding Open Access funding enabled and organized by Projekt DEAL.

Data availability All data that support the findings of this study are available upon reasonable request. The relevant source code is being reorganized in an open-source Julia repository named JYNAMICS.JL and a Python one named PYNACHAOS.

Appendix A: High-order shifts of periodic orbits and high-order shift progression of general orbits

In the main text, a simple deduction for $\delta \boldsymbol{x}_{\text{cyc}}$ is presented with only $\delta\mathcal{P}^m$ and $\mathcal{DP}^m$ involved. With higher order effects taken into account, Eq. (12) is complicated into Eq. (A1) as shown below and in Fig. 6,

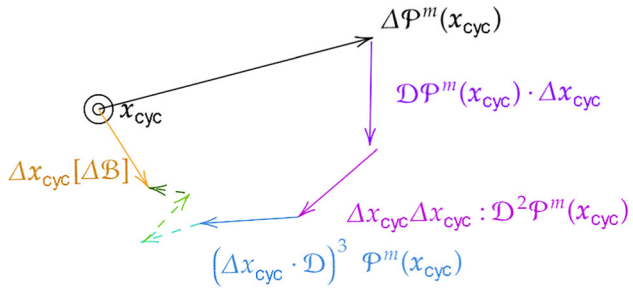

Fig. 6 Cartoon to show how to calculate the shift of a periodic point for a map under perturbation with high-order effects considered

$$\begin{aligned}
\Delta\mathbf{x}_{\rm cyc} &= \Delta\mathcal{P}^m(\mathbf{x}_{\rm cyc}) + \mathcal{D}\mathcal{P}^m(\mathbf{x}_{\rm cyc})\cdot\Delta\mathbf{x}_{\rm cyc}, \qquad \text{(12 revisited)}\\
\Delta\mathbf{x}_{\rm cyc} &= \Delta\mathcal{P}^m(\mathbf{x}_{\rm cyc}) + \left(\Delta\mathbf{x}_{\rm cyc}\cdot\mathcal{D}\right)\mathcal{P}^m(\mathbf{x}_{\rm cyc})\\
&\quad + \frac{1}{2!}\left(\Delta\mathbf{x}_{\rm cyc}\Delta\mathbf{x}_{\rm cyc}:\mathcal{D}^2\right)\mathcal{P}^m(\mathbf{x}_{\rm cyc})\cdots\\
&= \Delta\mathcal{P}^m(\mathbf{x}_{\rm cyc}) + \sum_{k=1}^{\infty}\left(\Delta\mathbf{x}_{\rm cyc}^k\vdots_{(k)}\mathcal{D}^k\right)\mathcal{P}^m(\mathbf{x}_{\rm cyc}),
\end{aligned} \tag{A1}$$

where $\Delta\boldsymbol{x}_{\rm cyc}^k\vdots_{(k)}\mathcal{D}^k := (\Delta\boldsymbol{x}_{\rm cyc}\cdot\mathcal{D})^k$ Expand $\Delta\boldsymbol{x}_{\rm cyc}$ and $\Delta\mathcal{P}^m$ by their variations of different orders:

$$\begin{aligned}
\Delta\boldsymbol{x}_{\rm cyc} &= \delta\boldsymbol{x}_{\rm cyc} + \frac{1}{2!}\delta^2\boldsymbol{x}_{\rm cyc} + \frac{1}{3!}\delta^3\boldsymbol{x}_{\rm cyc} + \cdots,\\
\Delta\mathcal{P}^m &= \delta\mathcal{P}^m + \frac{1}{2!}\delta^2\mathcal{P}^m + \frac{1}{3!}\delta^3\mathcal{P}^m + \cdots
\end{aligned}$$

Similarly, $\mathcal{D}^k\mathcal{P}^m$ also needs to be expanded:

$$\mathcal{D}^k\mathcal{P}^m[\mathcal{P}+\Delta\mathcal{P}](\boldsymbol{x}_{\rm cyc}[\mathcal{P}]) = \mathcal{D}^k\mathcal{P}^m[\mathcal{P}](\boldsymbol{x}_{\rm cyc}) + \delta\mathcal{D}^k\mathcal{P}^m[\mathcal{P};\Delta\mathcal{P}](\boldsymbol{x}_{\rm cyc}) + \frac{1}{2!}\delta^2\mathcal{D}^k\mathcal{P}^m[\mathcal{P};\Delta\mathcal{P},\ \Delta\mathcal{P}](\boldsymbol{x}_{\rm cyc}) + \cdots$$

Then to determine $\delta^k\boldsymbol{x}_{\rm cyc}$, collect terms in Eq. (A1) that contain an equal number of variations, denoted by k, to construct the equation of $k^{\rm th}$ order. Each functional variation $\delta^{k'}$ of order k' contributes k' to this count. For example, the first four orders equations are

$$\begin{aligned}
\delta\mathbf{x}_{\rm cyc} &= \delta\mathcal{P}^m + \delta\mathbf{x}_{\rm cyc}\cdot\mathcal{D}\mathcal{P}^m,\\
\frac{1}{2!}\delta^2\mathbf{x}_{\rm cyc} &= \frac{1}{2!}\delta^2\mathcal{P}^m + \frac{1}{2!}\delta^2\mathbf{x}_{\rm cyc}\cdot\mathcal{D}\mathcal{P}^m + \delta\mathbf{x}_{\rm cyc}\cdot\delta\mathcal{D}\mathcal{P}^m\\
&\quad + \frac{1}{2!}\delta\mathbf{x}_{\rm cyc}\delta\mathbf{x}_{\rm cyc}:\mathcal{D}^2\mathcal{P}^m,
\end{aligned} \tag{A2}$$

$$\begin{aligned}
\frac{1}{3!}\delta^3\mathbf{x}_{\rm cyc} &= \frac{1}{3!}\delta^3\mathcal{P}^m + \frac{1}{3!}\delta^3\mathbf{x}_{\rm cyc}\cdot\mathcal{D}\mathcal{P}^m + \frac{1}{2!}\delta^2\mathbf{x}_{\rm cyc}\cdot\frac{1}{1!}\delta\mathcal{D}\mathcal{P}^m\\
&\quad + \frac{1}{1!}\delta\mathbf{x}_{\rm cyc}\cdot\frac{1}{2!}\delta^2\mathcal{D}\mathcal{P}^m + \frac{1}{2!}\frac{1\times2}{2!}\delta^2\mathbf{x}_{\rm cyc}\delta\mathbf{x}_{\rm cyc}:\mathcal{D}^2\mathcal{P}^m\\
&\quad + \frac{1}{2!}\delta\mathbf{x}_{\rm cyc}\delta\mathbf{x}_{\rm cyc}:\delta\mathcal{D}^2\mathcal{P}^m + \frac{1}{3!}\delta\mathbf{x}_{\rm cyc}\delta\mathbf{x}_{\rm cyc}\delta\mathbf{x}_{\rm cyc}\vdots\mathcal{D}^3\mathcal{P}^m,
\end{aligned} \tag{A3}$$

$$\begin{aligned}
\frac{1}{4!}\delta^4\mathbf{x}_{\rm cyc} &= \frac{1}{4!}\delta^4\mathcal{P}^m + \frac{1}{4!}\delta^4\mathbf{x}_{\rm cyc}\cdot\mathcal{D}\mathcal{P}^m + \frac{1}{3!}\delta^3\mathbf{x}_{\rm cyc}\cdot\delta\mathcal{D}\mathcal{P}^m\\
&\quad + \frac{1}{2!}\delta^2\mathbf{x}_{\rm cyc}\cdot\frac{1}{2!}\delta^2\mathcal{D}\mathcal{P}^m + \frac{1}{1!}\delta\mathbf{x}_{\rm cyc}\cdot\frac{1}{3!}\delta^3\mathcal{D}\mathcal{P}^m\\
&\quad + \frac{1}{2!}\frac{1\times2}{3!}\delta^3\mathbf{x}_{\rm cyc}\delta\mathbf{x}_{\rm cyc}:\mathcal{D}^2\mathcal{P}^m + \frac{1}{2!}\frac{1}{2!}\delta^2\mathbf{x}_{\rm cyc}\frac{1}{2!}\delta^2\mathbf{x}_{\rm cyc}:\mathcal{D}^2\mathcal{P}^m\\
&\quad + \frac{1}{2!}\frac{2}{2!}\delta^2\mathbf{x}_{\rm cyc}\delta\mathbf{x}_{\rm cyc}:\delta\mathcal{D}^2\mathcal{P}^m + \frac{1}{2!}\delta\mathbf{x}_{\rm cyc}\delta\mathbf{x}_{\rm cyc}:\frac{1}{2!}\delta^2\mathcal{D}^2\mathcal{P}^m\\
&\quad + \frac{1}{3!}\frac{3}{2!}\delta^2\mathbf{x}_{\rm cyc}\delta\mathbf{x}_{\rm cyc}\delta\mathbf{x}_{\rm cyc}\vdots\mathcal{D}^3\mathcal{P}^m + \frac{1}{3!}\delta\mathbf{x}_{\rm cyc}\delta\mathbf{x}_{\rm cyc}\delta\mathbf{x}_{\rm cyc}:\delta\mathcal{D}^3\mathcal{P}^m\\
&\quad + \frac{1}{4!}\delta\mathbf{x}_{\rm cyc}\delta\mathbf{x}_{\rm cyc}\delta\mathbf{x}_{\rm cyc}\delta\mathbf{x}_{\rm cyc}\vdots_{(4)}\mathcal{D}^4\mathcal{P}^m,
\end{aligned} \tag{A4}$$

From the pattern of terms appearing in the above equations, one can conclude the n^{th} order formula for the shift of a periodic orbit as below,

$$\frac{1}{n!}\delta^n\mathbf{x}_{\text{cyc}} = \sum_{\substack{(p_i),(n_i),n_{\mathcal{P}} \text{ such that} \\ n_1p_1+\cdots+n_dp_d+n_{\mathcal{P}}=n}} \binom{p^+}{p_1,\ldots,p_d} (\frac{1}{n_1!}\delta^{n_1}\mathbf{x}_{\text{cyc}})^{p_1}\cdots(\frac{1}{n_d!}\delta^{n_d}\mathbf{x}_{\text{cyc}})^{p_d} \vdots_{(p^+)} \frac{\delta^{n_{\mathcal{P}}}\mathcal{D}^{p^+}\mathcal{P}^m}{n_{\mathcal{P}}!p^+!} \tag{A5}$$

where

$$\begin{aligned} &p_i \geq 1, \qquad n_1 > n_2 > \cdots > n_d \geq 1, \\ &p^+ := p_1 + p_2 + \cdots + p_d, \quad d\text{is the number of powers}, \\ &n \geq p^+ \geq 0, \qquad \text{and } n_{\mathcal{P}} \geq 0. \end{aligned}$$

Note that on the RHS of Eq. (A5), there exists a term containing $\delta^n\boldsymbol{x}_{\text{cyc}}$, that is

$$\delta^n\boldsymbol{x}_{\text{cyc}} \cdot \mathcal{D}\mathcal{P}^m/n!\,.$$

To solve for $\delta^n\boldsymbol{x}_{\text{cyc}}$, one needs to move this term to LHS and multiply both sides by a matrix, $-n!\,(\mathcal{D}\mathcal{P}^m - \mathbf{I})^{-1}$.

One can also directly impose $\Delta\mathcal{B}\cdot\mathrm{d}/\mathrm{d}\mathcal{B}$ on both sides of the equation of order k to acquire the equation of order $k+1$ recursively. For example, the equation of second order can be deduced from that of first-order

$$\delta\boldsymbol{x}_{\text{cyc}} = -(\mathcal{D}\mathcal{P}^m - \mathbf{I})^{-1}\delta\mathcal{P}^m. \qquad (14 revisited)$$

Keep in mind that for a matrix-valued function $\mathbf{A}(x)$, $(\mathbf{A}^{-1})' = -\mathbf{A}^{-1}\mathbf{A}'\mathbf{A}^{-1}$. This identity is employed several times in this paper.

$$\begin{aligned} \delta^2\boldsymbol{x}_{\text{cyc}} = (\mathcal{D}\mathcal{P}^m - \mathbf{I})^{-1} \quad & \underbrace{(\Delta\mathcal{B}\cdot\frac{\mathrm{d}}{\mathrm{d}\mathcal{B}})\mathcal{D}\mathcal{P}^m}_{=\delta\boldsymbol{x}_{\text{cyc}}\cdot\mathcal{D}^2\mathcal{P}^m+\delta\mathcal{D}\mathcal{P}^m} \quad \underbrace{(\mathcal{D}\mathcal{P}^m - \mathbf{I})^{-1}\delta\mathcal{P}^m}_{=-\delta\boldsymbol{x}_{\text{cyc}}} \\ - (\mathcal{D}\mathcal{P}^m - \mathbf{I})^{-1} \quad & \underbrace{(\Delta\mathcal{B}\cdot\frac{\mathrm{d}}{\mathrm{d}\mathcal{B}})\delta\mathcal{P}^m}_{\delta^2\mathcal{P}^m+\delta\boldsymbol{x}_{\text{cyc}}\cdot\delta\mathcal{D}\mathcal{P}^m}\,. \end{aligned} \tag{A6}$$

Since $\mathcal{P}^m$ here is evaluated at the periodic point $\boldsymbol{x}_{\text{cyc}}$ (obviously dependent on $\mathcal{B}$), the directional functional derivative $\Delta\mathcal{B}\cdot\mathrm{d}/\mathrm{d}\mathcal{B}$ imposed on $\delta^{k_\delta}\mathcal{D}^{k_D}\mathcal{P}^m$ not only brings a term $\delta^{k_\delta+1}\mathcal{D}^{k_D}\mathcal{P}^m$ but also $\delta\boldsymbol{x}_{\text{cyc}}\cdot\delta^{k_\delta}\mathcal{D}^{k_D+1}\mathcal{P}^m$. Equations (A2) and (A6) derived via two approaches lead to the same result:

$$\delta^2\boldsymbol{x}_{\text{cyc}} = -(\mathcal{D}\mathcal{P}^m - \mathbf{I})^{-1}\big(\delta^2\mathcal{P}^m + 2\delta\boldsymbol{x}_{\text{cyc}}\cdot\delta\mathcal{D}\mathcal{P}^m + \delta\boldsymbol{x}_{\text{cyc}}\delta\boldsymbol{x}_{\text{cyc}} : \mathcal{D}^2\mathcal{P}^m\big), \tag{A7}$$

which can be further imposed $\Delta\mathcal{B}\cdot\mathrm{d}/\mathrm{d}\mathcal{B}$ on both sides to acquire expressions for the third and fourth orders as shown below. They can be easily checked to be consistent with Eqs. (A3) and (A4) by comparing the coefficients.

$$\begin{aligned} \delta^3\mathbf{x}_{\text{cyc}} = &-(\mathcal{D}\mathcal{P}^m - \mathbf{I})^{-1} - (\Delta\mathcal{B}\cdot\frac{\mathrm{d}}{\mathrm{d}\mathcal{B}})(\mathcal{D}\mathcal{P}^m - \mathbf{I})\overbrace{(\mathcal{D}\mathcal{P}^m - \mathbf{I})^{-1}\left(\delta^2\mathcal{P}^m + 2\delta\mathbf{x}_{\text{cyc}}\cdot\delta\mathcal{D}\mathcal{P}^m + \delta\mathbf{x}_{\text{cyc}}\delta\mathbf{x}_{\text{cyc}} : \mathcal{D}^2\mathcal{P}^m\right)}^{-\delta^2\mathbf{x}_{\text{cyc}}} \\ &- (\mathcal{D}\mathcal{P}^m - \mathbf{I})^{-1}\Big(\delta\mathbf{x}_{\text{cyc}}\cdot\delta^2\mathcal{D}\mathcal{P}^m + \delta^3\mathcal{P}^m + 2\delta^2\mathbf{x}_{\text{cyc}}\cdot\delta\mathcal{D}\mathcal{P}^m + 2\delta\mathbf{x}_{\text{cyc}}\delta\mathbf{x}_{\text{cyc}} : \delta\mathcal{D}^2\mathcal{P}^m + 2\delta\mathbf{x}_{\text{cyc}}\cdot\delta^2\mathcal{D}\mathcal{P}^m \\ &+ 2\delta^2\mathbf{x}_{\text{cyc}}\delta\mathbf{x}_{\text{cyc}} : \mathcal{D}^2\mathcal{P}^m + \delta\mathbf{x}_{\text{cyc}}\delta\mathbf{x}_{\text{cyc}}\delta\mathbf{x}_{\text{cyc}} \vdots \mathcal{D}^3\mathcal{P}^m + \delta\mathbf{x}_{\text{cyc}}\delta\mathbf{x}_{\text{cyc}} : \delta\mathcal{D}^2\mathcal{P}^m\Big) \end{aligned} \tag{A8}$$

$$\begin{aligned} = &-(\mathcal{D}\mathcal{P}^m - \mathbf{I})^{-1}\Big(\delta^3\mathcal{P}^m + 3\delta^2\mathbf{x}_{\text{cyc}}\cdot\delta\mathcal{D}\mathcal{P}^m + 3\delta\mathbf{x}_{\text{cyc}}\delta\mathbf{x}_{\text{cyc}} : \delta\mathcal{D}^2\mathcal{P}^m \\ &+ 3\delta\mathbf{x}_{\text{cyc}}\cdot\delta^2\mathcal{D}\mathcal{P}^m + 3\delta^2\mathbf{x}_{\text{cyc}}\delta\mathbf{x}_{\text{cyc}} : \mathcal{D}^2\mathcal{P}^m + \delta\mathbf{x}_{\text{cyc}}\delta\mathbf{x}_{\text{cyc}}\delta\mathbf{x}_{\text{cyc}} \vdots \mathcal{D}^3\mathcal{P}^m\Big) \end{aligned} \tag{A9}$$

$$\begin{aligned}\delta^4\mathbf{x}_{\rm cyc} = -(\mathcal{D}\mathcal{P}^m - \mathbf{I})^{-1}\Big(&\delta^4\mathcal{P}^m + 4\delta^3\mathbf{x}_{\rm cyc}\cdot\delta\mathcal{D}\mathcal{P}^m + 6\delta^2\mathbf{x}_{\rm cyc}\cdot\delta^2\mathcal{D}\mathcal{P}^m + 6\delta\mathbf{x}_{\rm cyc}\delta\mathbf{x}_{\rm cyc}:\delta^2\mathcal{D}^2\mathcal{P}^m\\ &+4\delta\mathbf{x}_{\rm cyc}\cdot\delta^3\mathcal{D}\mathcal{P}^m + 4\delta^3\mathbf{x}_{\rm cyc}\delta\mathbf{x}_{\rm cyc}:\mathcal{D}^2\mathcal{P}^m + 6\delta^2\mathbf{x}_{\rm cyc}\delta\mathbf{x}_{\rm cyc}\delta\mathbf{x}_{\rm cyc}\vdots\mathcal{D}^3\mathcal{P}^m + 12\delta^2\mathbf{x}_{\rm cyc}\delta\mathbf{x}_{\rm cyc}:\delta\mathcal{D}^2\mathcal{P}^m\\ &+3\delta^2\mathbf{x}_{\rm cyc}\delta^2\mathbf{x}_{\rm cyc}:\mathcal{D}^2\mathcal{P}^m + 4\delta\mathbf{x}_{\rm cyc}\delta\mathbf{x}_{\rm cyc}\delta\mathbf{x}_{\rm cyc}\vdots\delta\mathcal{D}^3\mathcal{P}^m + \delta\mathbf{x}_{\rm cyc}\delta\mathbf{x}_{\rm cyc}\delta\mathbf{x}_{\rm cyc}\delta\mathbf{x}_{\rm cyc}\vdots_{(4)}\mathcal{D}^4\mathcal{P}^m\Big)\end{aligned} \tag{A10}$$

Similarly, the progression of general trajectory variations such as those of the first three orders is described by Eqs. (6a),(7),(8). One can obtain the $n^{\rm th}$ order trajectory variation progression formula as below in a manner similar to the formula (A5),

$$\begin{aligned}\frac{1}{n!}\frac{\partial}{\partial t}\delta^n\mathbf{X} = &\sum_{\substack{(n_i),(p_i),n_{\mathbf{B}}\ \text{such that}\\ n_1p_1+\cdots+n_dp_d+n_{\mathbf{B}}=n}}\binom{p^+}{p_1,\ldots,p_d}\\ &\cdot(\frac{1}{n_1!}\delta^{n_1}\mathbf{X})^{p_1}\cdots(\frac{1}{n_d!}\delta^{n_d}\mathbf{X})^{p_d}\vdots_{(p^+)}\frac{1}{p^+!n_{\mathbf{B}}!}\nabla^{p^+}\delta^{n_{\mathbf{B}}}\mathbf{B},\end{aligned} \tag{A11}$$

where

$$\begin{aligned}&p_i \geq 1, \qquad n_1 > n_2 > \cdots > n_d \geq 1,\\ &p^+ := p_1 + p_2 + \cdots + p_d, \quad d\text{is the number of powers},\\ &n \geq p^+ \geq 0, \quad \text{and } n_{\boldsymbol{B}} \geq 0.\end{aligned}$$

The formula (A11) can be easily migrated from N-D continuous-time flows to N-D discrete-time maps, e.g., $\mathcal{P}$, to describe the progression of discrete orbit variations by substituting symbols as below

$$\begin{aligned}\frac{\partial}{\partial t}\boldsymbol{X}(\boldsymbol{x}_0,t)\ \text{on LHS} &\mapsto \boldsymbol{X}(\boldsymbol{x}_0,k+1) = \mathcal{P}^{k+1}(\boldsymbol{x}_0),\\ \boldsymbol{X}(\boldsymbol{x}_0,t)\ \text{on RHS} &\mapsto \boldsymbol{X}(\boldsymbol{x}_0,k) = \mathcal{P}^{k}(\boldsymbol{x}_0),\ ,\\ \boldsymbol{B} &\mapsto \mathcal{P},\\ \nabla\boldsymbol{B} &\mapsto \mathcal{D}\mathcal{P}.\end{aligned}$$

Appendix B: Evolution of the cycle shift along a cycle

As stated in the main text, the evolution of the perpendicular shift of a cycle, $\delta_\perp\boldsymbol{x}_{\rm cyc}$, along a cycle is too verbose to be called a formula. The deduction details are shown below.

$$\delta_\perp\boldsymbol{x}_{\rm cyc} = \Big[\mathbf{I} - (\mathbf{I} - \hat{\boldsymbol{b}}\hat{\boldsymbol{b}}^T)\cdot\mathcal{D}\boldsymbol{X}_T\Big]^{-1}\cdot(\mathbf{I} - \hat{\boldsymbol{b}}\hat{\boldsymbol{b}}^T)\cdot\delta\boldsymbol{X}_T \qquad (15\ \textit{revisited})$$

with both sides differentiated in t converts to

$$\begin{aligned}\frac{\mathrm{d}}{\mathrm{d}t}\delta_\perp\boldsymbol{x}_{\rm cyc} = &\frac{\mathrm{d}}{\mathrm{d}t}\Big[\mathbf{I} - (\mathbf{I} - \hat{\boldsymbol{b}}\hat{\boldsymbol{b}}^T)\cdot\mathcal{D}\boldsymbol{X}_T\Big]^{-1}\cdot(\mathbf{I} - \hat{\boldsymbol{b}}\hat{\boldsymbol{b}}^T)\cdot\delta\boldsymbol{X}_T\\ &+\Big[\mathbf{I} - (\mathbf{I} - \hat{\boldsymbol{b}}\hat{\boldsymbol{b}}^T)\cdot\mathcal{D}\boldsymbol{X}_T\Big]^{-1}\cdot\frac{\mathrm{d}}{\mathrm{d}t}(\mathbf{I} - \hat{\boldsymbol{b}}\hat{\boldsymbol{b}}^T)\cdot\delta\boldsymbol{X}_T\\ &+\Big[\mathbf{I} - (\mathbf{I} - \hat{\boldsymbol{b}}\hat{\boldsymbol{b}}^T)\cdot\mathcal{D}\boldsymbol{X}_T\Big]^{-1}\cdot(\mathbf{I} - \hat{\boldsymbol{b}}\hat{\boldsymbol{b}}^T)\cdot\frac{\mathrm{d}}{\mathrm{d}t}\delta\boldsymbol{X}_T\end{aligned} \tag{B1}$$

$$\begin{aligned}= -&\Big[\mathbf{I} - (\mathbf{I} - \hat{\boldsymbol{b}}\hat{\boldsymbol{b}}^T)\cdot\mathcal{D}\boldsymbol{X}_T\Big]^{-1}\cdot\frac{\mathrm{d}}{\mathrm{d}t}\Big[\mathbf{I} - (\mathbf{I} - \hat{\boldsymbol{b}}\hat{\boldsymbol{b}}^T)\cdot\mathcal{D}\boldsymbol{X}_T\Big]\\ &\bullet\underbrace{\Big[\mathbf{I} - (\mathbf{I} - \hat{\boldsymbol{b}}\hat{\boldsymbol{b}}^T)\cdot\mathcal{D}\boldsymbol{X}_T\Big]^{-1}\cdot(\mathbf{I} - \hat{\boldsymbol{b}}\hat{\boldsymbol{b}}^T)\cdot\delta\boldsymbol{X}_T}_{=\delta_\perp\boldsymbol{x}_{\rm cyc}}\end{aligned}$$

$$+\left[\mathbf{I}-(\mathbf{I}-\hat{\boldsymbol{b}}\hat{\boldsymbol{b}}^T)\cdot\mathcal{D}\boldsymbol{X}_T\right]^{-1}\cdot\frac{\mathrm{d}}{\mathrm{d}t}(\mathbf{I}-\hat{\boldsymbol{b}}\hat{\boldsymbol{b}}^T)\cdot\delta\boldsymbol{X}_T$$
$$+\left[\mathbf{I}-(\mathbf{I}-\hat{\boldsymbol{b}}\hat{\boldsymbol{b}}^T)\cdot\mathcal{D}\boldsymbol{X}_T\right]^{-1}\cdot(\mathbf{I}-\hat{\boldsymbol{b}}\hat{\boldsymbol{b}}^T)\cdot\frac{\mathrm{d}}{\mathrm{d}t}\delta\boldsymbol{X}_T \tag{B2}$$

where $\frac{\mathrm{d}}{\mathrm{d}t}(\mathbf{I}-\hat{\boldsymbol{b}}\hat{\boldsymbol{b}}^T)=-\boldsymbol{B}\cdot\nabla(\hat{\boldsymbol{b}}\hat{\boldsymbol{b}}^T)=-B(\boldsymbol{\kappa}\hat{\boldsymbol{b}}^T+\hat{\boldsymbol{b}}\hat{\boldsymbol{\kappa}}^T)$, while $\frac{\mathrm{d}}{\mathrm{d}t}\delta\boldsymbol{X}_T=\mathbf{A}\ \delta\boldsymbol{X}_T-(\mathcal{D}\boldsymbol{X}_T-\mathbf{I})\delta\boldsymbol{B}$, which is Eq. (17a) in the main text. Even though these two derivatives have clear expressions, the RHS seems hard to reduce further.

In contrast, the full variation $\delta\boldsymbol{x}_{\mathrm{cyc}}$—including both the parallel and perpendicular components—has a concise formula to evolve along a cycle, that is Eq. (18a) in N-D cases and Eq. (18b) in cylindrical coordinates in 3D cases. Without loss of generality, it is shown below the proof of the evolution formula for the latter cylindrical case,

$$\frac{\mathrm{d}}{\mathrm{d}\phi}\delta\boldsymbol{x}_{\mathrm{cyc}}=\frac{\partial(R\boldsymbol{B}_{\mathrm{pol}}/B_\phi)}{\partial(R,\,Z)}\cdot\delta\boldsymbol{x}_{\mathrm{cyc}}+\delta\frac{R\boldsymbol{B}_{\mathrm{pol}}}{B_\phi}. \qquad \text{18b revisited}$$

Proof Differentiate both sides of Eq. (14) *w.r.t.* ϕ, then

$$\frac{\mathrm{d}}{\mathrm{d}\phi}\delta\boldsymbol{x}_{\mathrm{cyc}}=-\underbrace{\frac{\mathrm{d}}{\mathrm{d}\phi}[\mathcal{D}\mathcal{P}^m-\mathbf{I}]^{-1}}_{\substack{\text{utilize the identity}\\ (\mathbf{A}^{-1})'=\mathbf{A}^{-1}(-\mathbf{A}')\mathbf{A}^{-1}\\ \text{for a matrix-valued function}\mathbf{A}}}\cdot\delta\mathcal{P}^m-[\mathcal{D}\mathcal{P}^m-\mathbf{I}]^{-1}\cdot\frac{\mathrm{d}}{\mathrm{d}\phi}\delta\mathcal{P}^m$$
$$=-[\mathcal{D}\mathcal{P}^m-\mathbf{I}]^{-1}(-\frac{\mathrm{d}}{\mathrm{d}\phi}\mathcal{D}\mathcal{P}^m)[\mathcal{D}\mathcal{P}^m-\mathbf{I}]^{-1}\cdot\delta\mathcal{P}^m$$
$$-[\mathcal{D}\mathcal{P}^m-\mathbf{I}]^{-1}\cdot\frac{\mathrm{d}}{\mathrm{d}\phi}\delta\mathcal{P}^m$$
$$=-[\mathcal{D}\mathcal{P}^m-\mathbf{I}]^{-1}\cdot\left((-\frac{\mathrm{d}}{\mathrm{d}\phi}\mathcal{D}\mathcal{P}^m)[\mathcal{D}\mathcal{P}^m-\mathbf{I}]^{-1}\cdot\delta\mathcal{P}^m+\frac{\mathrm{d}}{\mathrm{d}\phi}\delta\mathcal{P}^m\right)$$

[note that $\frac{\mathrm{d}}{\mathrm{d}\phi}\mathcal{D}\mathcal{P}^m=\mathbf{A}\cdot\mathcal{D}\mathcal{P}^m-\mathcal{D}\mathcal{P}^m\cdot\mathbf{A}$ by Eq. (3b) and the expression for $\frac{\mathrm{d}}{\mathrm{d}\phi}\delta\mathcal{P}^m$ can be found in Eq. (17b)]

$$=-\mathbf{A}[\mathcal{D}\mathcal{P}^m-\mathbf{I}]^{-1}\cdot\delta\mathcal{P}^m+\delta\frac{R\boldsymbol{B}_{\mathrm{pol}}}{B_\phi}$$
$$=\mathbf{A}\delta\boldsymbol{x}_{\mathrm{cyc}}+\delta\frac{R\boldsymbol{B}_{\mathrm{pol}}}{B_\phi}$$

Appendix C: $(\Delta\mathcal{B}\cdot\mathrm{d}/\mathrm{d}\mathcal{B})\ \mathcal{D}\mathcal{P}^m$ The change of full-period Jacobian

For the full-period Jacobian of a cycle and its change under perturbation discussed in the main text, the derivation and detailed formulae are shown here. As a first step, with the whole system $\mathcal{B}$ considered as an argument, the $\mathcal{D}\boldsymbol{X}_{\mathrm{pol}}$ progression equation $\partial_{\phi_{\mathrm{e}}}\mathcal{D}\boldsymbol{X}_{\mathrm{pol}}(\boldsymbol{x}_{0,\,\mathrm{pol}},\,\phi_{\mathrm{s}},\,\phi_{\mathrm{e}})=\mathbf{A}\bullet\mathcal{D}\boldsymbol{X}_{\mathrm{pol}}$, Eq. (2b) in the main text, is complicated into

$$\frac{\partial}{\partial\phi_{\mathrm{e}}}\mathcal{D}\boldsymbol{X}_{\mathrm{pol}}[\mathcal{B}](\boldsymbol{x}_{\mathrm{cyc}}[\mathcal{B}](\phi_{\mathrm{s}}),\,\phi_{\mathrm{s}},\,\phi_{\mathrm{e}})$$
$$=\mathbf{A}[\mathcal{B}](\boldsymbol{x}_{\mathrm{cyc}}[\mathcal{B}](\phi_{\mathrm{e}}),\,\phi_{\mathrm{e}})\bullet\mathcal{D}\boldsymbol{X}_{\mathrm{pol}}[\mathcal{B}](\boldsymbol{x}_{\mathrm{cyc}}[\mathcal{B}](\phi_{\mathrm{s}}),\,\phi_{\mathrm{s}},\,\phi_{\mathrm{e}}), \tag{C1}$$

which after imposed $\Delta\mathcal{B}\cdot\frac{\mathrm{d}}{\mathrm{d}\mathcal{B}}\mathcal{B}$ converts to

$$\frac{\partial}{\partial\phi_{\mathrm{e}}}(\Delta\mathcal{B}\cdot\frac{\mathrm{d}}{\mathrm{d}\mathcal{B}})\mathcal{D}\mathbf{X}_{\mathrm{pol}}[\mathcal{B}](\mathbf{x}_{\mathrm{cyc}}[\mathcal{B}](\phi_{\mathrm{s}}),\phi_{\mathrm{s}},\phi_{\mathrm{e}})=$$
$$\mathbf{A}\bullet\left(\Delta\mathcal{B}\cdot\frac{\mathrm{d}}{\mathrm{d}\mathcal{B}}\right)\mathcal{D}\mathbf{X}_{\mathrm{pol}}+\left(\Delta\mathcal{B}\cdot\frac{\delta}{\delta\mathcal{B}}+\left(\Delta\mathcal{B}\cdot\frac{\delta\mathbf{x}_{\mathrm{cyc}}[\mathcal{B}](\phi_{\mathrm{e}})}{\delta\mathcal{B}}\right)\cdot\frac{\partial}{\partial(R,Z)}\right)\left(\mathbf{A}[\mathcal{B}](\mathbf{x}_{\mathrm{cyc}}[\mathcal{B}](\phi_{\mathrm{e}}),\phi_{\mathrm{e}})\right)\bullet\mathcal{D}\mathbf{X}_{\mathrm{pol}} \tag{C2}$$

giving $(\Delta\mathcal{B}\cdot\frac{\mathrm{d}}{\mathrm{d}\mathcal{B}})\mathcal{D}\boldsymbol{X}_{\mathrm{pol}}$ on LHS after an integration in ϕ_{e}. The arrows appearing in this equation, respectively, point from a derivative notation to the corresponding argument upon which the derivative is to operate. Note that $(\Delta\mathcal{B}\cdot\frac{\mathrm{d}}{\mathrm{d}\mathcal{B}})\mathcal{D}\boldsymbol{X}_{\mathrm{pol}}$ is a total functional derivative considering $\boldsymbol{x}_{\mathrm{cyc}}$ shift. Furthermore, to avoid repeated computation for $(\Delta\mathcal{B}\cdot\frac{\mathrm{d}}{\mathrm{d}\mathcal{B}})\mathcal{D}\boldsymbol{X}_{\mathrm{pol}}$ at all ϕ-sections, one can similarly process the $\mathcal{DP}^m$ evolution formula $\frac{\mathrm{d}}{\mathrm{d}\phi}\,\mathcal{DP}^m=\left[\mathbf{A},\,\mathcal{DP}^m\right]$ to let the $\mathcal{B}$ argument be explicit,

$$\begin{aligned}&\frac{\mathrm{d}}{\mathrm{d}\phi}\mathcal{DP}^m[\mathcal{B}](\boldsymbol{x}_{\mathrm{cyc}}[\mathcal{B}](\phi),\,\phi)\\&=\Big[\mathbf{A}[\mathcal{B}](\boldsymbol{x}_{\mathrm{cyc}}[\mathcal{B}](\phi),\,\phi),\quad\mathcal{DP}^m[\mathcal{B}](\boldsymbol{x}_{\mathrm{cyc}}[\mathcal{B}](\phi),\,\phi)\Big],\end{aligned}\tag{C3}$$

which after imposed $\Delta\mathcal{B}\cdot\mathrm{d}/\mathrm{d}\mathcal{B}$ on both sides becomes,

$$\begin{aligned}&\tfrac{\mathrm{d}}{\mathrm{d}\phi}(\Delta\mathcal{B}\cdot\tfrac{\mathrm{d}}{\mathrm{d}\mathcal{B}})\,\mathcal{DP}^m[\mathcal{B}](\mathbf{x}_{\mathrm{cyc}}[\mathcal{B}](\phi),\phi)=\\&\Big[\mathbf{A},\;\Big(\Delta\mathcal{B}\cdot\tfrac{\mathrm{d}}{\mathrm{d}\mathcal{B}}\Big)\mathcal{DP}^m\Big]+\Big[\Big(\Delta\mathcal{B}\cdot\underbrace{\tfrac{\delta}{\delta\mathcal{B}}+\Big(\Delta\mathcal{B}\cdot\tfrac{\delta\mathbf{x}_{\mathrm{cyc}}[\mathcal{B}](\phi)}{\delta\mathcal{B}}\Big)\cdot\tfrac{\partial}{\partial(R,Z)}}\Big)\mathbf{A}[\mathcal{B}](\mathbf{x}_{\mathrm{cyc}}[\mathcal{B}](\phi),\phi),\;\mathcal{DP}^m\Big],\end{aligned}\tag{C4}$$

of which an integration in ϕ yields $(\Delta\mathcal{B}\cdot\frac{\mathrm{d}}{\mathrm{d}\mathcal{B}})\mathcal{DP}^m$ on all sections. The initial condition of this matrix ODE system is $(\Delta\mathcal{B}\cdot\frac{\mathrm{d}}{\mathrm{d}\mathcal{B}})\mathcal{D}\boldsymbol{X}_{\mathrm{pol}}(\phi_{\mathrm{s}},\,\phi_{\mathrm{e}}=\phi_{\mathrm{s}}+2m\pi)$, coming from a $2m\pi$ integration in ϕ_{e} of Eq. (C2).

Only the second term on the RHS of Eq. (C2), that is $(\Delta\mathcal{B}\cdot\delta/\delta\mathcal{B})\;\mathbf{A}$, may need to be explained to readers. The other terms are comparatively easy to handle. Components of it are shown in a matrix form

$$(\Delta\mathcal{B}\cdot\frac{\delta}{\delta\mathcal{B}})\;\mathbf{A}[\mathcal{B}](\boldsymbol{x}_{\mathrm{cyc}}[\mathcal{B}](\phi_{\mathrm{s}}),\,\phi_{\mathrm{s}},\,\phi_{\mathrm{e}})\tag{C5}$$

(Note that $\delta/\delta\mathcal{B}$ is a partial derivative, so $\boldsymbol{x}_{\mathrm{cyc}}$ does not matter here.)

$$\begin{aligned}&=(\Delta\mathcal{B}\cdot\frac{\delta}{\delta\mathcal{B}})\begin{bmatrix}\frac{B_R}{B_\phi}+R\Big(\frac{\partial_R B_R}{B_\phi}-\frac{B_R\partial_R B_\phi}{B_\phi^2}\Big) & R\Big(\frac{\partial_Z B_R}{B_\phi}-\frac{B_R\partial_Z B_\phi}{B_\phi^2}\Big)\\ \frac{B_Z}{B_\phi}+R\Big(\frac{\partial_R B_Z}{B_\phi}-\frac{B_Z\partial_R B_\phi}{B_\phi^2}\Big) & R\Big(\frac{\partial_Z B_Z}{B_\phi}-\frac{B_Z\partial_Z B_\phi}{B_\phi^2}\Big)\end{bmatrix}\\&=\begin{bmatrix}\frac{\delta B_R}{B_\phi}-\frac{B_R}{B_\phi^2}\delta B_\phi+(1,\,1)\;(1,\,2)\\ \frac{\delta B_Z}{B_\phi}-\frac{B_Z}{B_\phi^2}\delta B_\phi+(2,\,1)\;(2,\,2)\end{bmatrix}\\(1,\,1)&=R\Big(\frac{\partial_R\delta B_R}{B_\phi}-\frac{\partial_R B_R}{B_\phi^2}\delta B_\phi-\frac{\partial_R B_\phi}{B_\phi^2}\delta B_R\\&\qquad-B_R\frac{(\partial_R\delta B_\phi)B_\phi^2-(\partial_R B_\phi)2B_\phi\delta B_\phi}{B_\phi^4}\Big)\\(1,\,2)&=(1,\,1)\text{ with }\partial_R\text{ replaced by }\partial_Z.\\(2,\,1)&=(1,\,1)\text{ with }B_R\text{ and }\delta B_R\textit{resp.}\text{replaced by }B_Z\text{ and }\delta B_Z.\\(2,\,2)&=(1,\,1)\text{ with }\partial_R,\,B_R\text{ and }\delta B_R\textit{resp.}\text{replaced by }\partial_Z,\,B_Z\text{ and }\delta B_Z.\end{aligned}\tag{C6}$$

An alternative expression of $(\Delta\mathcal{B}\cdot\frac{\delta}{\delta\mathcal{B}})\;\mathbf{A}$ is acquired by calculating $(\Delta\mathcal{B}\cdot\frac{\delta}{\delta\mathcal{B}})$ first and then $\frac{\partial}{\partial(R,\,Z)}$, that is

$$\frac{\partial}{\partial(R,\,Z)}\left(\delta\frac{R\boldsymbol{B}_{\mathrm{pol}}}{B_\phi}\right)=\frac{\partial}{\partial(R,\,Z)}\left(\frac{R\delta\boldsymbol{B}_{\mathrm{pol}}}{B_\phi}-\frac{R\boldsymbol{B}_{\mathrm{pol}}}{B_\phi^2}\delta B_\phi\right).$$

To migrate Eqs. (C1–C4) from 3D flows in cylindrical coordinates to N-D flows in Cartesian coordinates, substitute symbols as below

$$\mathbf{A}\mapsto\nabla\boldsymbol{B},\mathcal{DP}^m\mapsto\mathcal{D}\boldsymbol{X}_T,\qquad\qquad\frac{\partial}{\partial(R,\,Z)}\mapsto\nabla.$$

Be aware that the perturbation may change the period of this cycle, so the change in the time integration range may bring new terms in these equations.

To migrate Eqs. (C1–C4) to N-D discrete maps, one needs more than symbol substitution. Simply denote a general map by $\mathcal{P}$. The counterpart of Jacobian progression Eq. (2b) for mapping is

$$\mathcal{DP}^k(\boldsymbol{x}) = \mathcal{DP}(\mathcal{P}^{k-1}(\boldsymbol{x})) \cdot \mathcal{DP}^{k-1}(\boldsymbol{x}) \tag{C7}$$

Given an m-periodic orbit $\{\boldsymbol{x}_{\rm cyc}, \mathcal{P}(\boldsymbol{x}_{\rm cyc}), \cdots, \mathcal{P}^{m-1}(\boldsymbol{x}_{\rm cyc})\}$, one can compare

$$\mathcal{DP}^m(\boldsymbol{x}_{\rm cyc}) = \mathcal{DP}(\mathcal{P}^{m-1}(\boldsymbol{x}_{\rm cyc})) \cdot \mathcal{DP}(\mathcal{P}^{m-2}(\boldsymbol{x}_{\rm cyc})) \cdots \mathcal{DP}(\boldsymbol{x}_{\rm cyc})$$

and

$$\mathcal{DP}^m(\mathcal{P}(\boldsymbol{x}_{\rm cyc})) = \mathcal{DP}(\mathcal{P}^{m}(\boldsymbol{x}_{\rm cyc})) \cdot \mathcal{DP}(\mathcal{P}^{m-1}(\boldsymbol{x}_{\rm cyc})) \cdots \mathcal{DP}(\mathcal{P}(\boldsymbol{x}_{\rm cyc}))$$

to find the relationship between $\mathcal{DP}^m(\boldsymbol{x}_{\rm cyc})$ and $\mathcal{DP}^m(\mathcal{P}(\boldsymbol{x}_{\rm cyc}))$, that is

$$\begin{aligned} \mathcal{DP}^m(\mathcal{P}(\boldsymbol{x}_{\rm cyc})) &= \mathcal{DP}(\mathcal{P}^m(\boldsymbol{x}_{\rm cyc})) \cdot \mathcal{DP}^m(\boldsymbol{x}_{\rm cyc}) \cdot [\mathcal{DP}(\boldsymbol{x}_{\rm cyc})]^{-1} \\ &= \mathcal{DP}(\boldsymbol{x}_{\rm cyc}) \cdot \mathcal{DP}^m(\boldsymbol{x}_{\rm cyc}) \cdot [\mathcal{DP}(\boldsymbol{x}_{\rm cyc})]^{-1}, \end{aligned} \tag{C8}$$

which is the counterpart of $\mathcal{DP}^m$ evolution formula (3b) for mapping. Upon applied $\Delta\mathcal{P} \cdot \frac{\rm d}{{\rm d}\mathcal{P}}$ on both sides, Eqs. (C7) and (C8) transform to the progression equation of $(\Delta\mathcal{P} \cdot \frac{\rm d}{{\rm d}\mathcal{P}})\mathcal{DP}^k(\boldsymbol{x}_{\rm cyc})$,

$$\begin{aligned} (\Delta\mathcal{P} \cdot \frac{\rm d}{{\rm d}\mathcal{P}})\mathcal{DP}^k(\boldsymbol{x}_{\rm cyc}) &= \mathcal{DP}(\mathcal{P}^{k-1}(\boldsymbol{x}_{\rm cyc})) \cdot (\Delta\mathcal{P} \cdot \frac{\rm d}{{\rm d}\mathcal{P}})\mathcal{DP}^{k-1}(\boldsymbol{x}_{\rm cyc}) \\ &+ \underbrace{(\Delta\mathcal{P} \cdot \frac{\rm d}{{\rm d}\mathcal{P}})\big[\mathcal{DP}(\mathcal{P}^{k-1}(\boldsymbol{x}_{\rm cyc}))\big]}\cdot\mathcal{DP}^{k-1}(\boldsymbol{x}_{\rm cyc}), \\ &= \delta\mathcal{DP}(\mathcal{P}^{k-1}(\boldsymbol{x}_{\rm cyc})) + \big[(\delta\mathcal{P}^{k-1} + \delta_{\boldsymbol{x}_{\rm cyc}} \cdot \mathcal{DP}^{k-1}) \cdot \mathcal{D}\big]\mathcal{DP}(\mathcal{P}^{k-1}(\boldsymbol{x}_{\rm cyc})) \end{aligned} \tag{C9}$$

and the evolution equation of $(\Delta\mathcal{P} \cdot \frac{\rm d}{{\rm d}\mathcal{P}})\mathcal{DP}^m(\boldsymbol{x}_{\rm cyc})$ along a discrete periodic orbit,

$$\begin{aligned} &(\Delta\mathcal{P} \cdot \frac{\rm d}{{\rm d}\mathcal{P}})\mathcal{DP}^m(\mathcal{P}(\boldsymbol{x}_{\rm cyc})) \\ &\overbrace{\qquad\qquad\qquad\qquad}^{=\delta\mathcal{DP}+(\delta\boldsymbol{x}_{\rm cyc}\cdot\mathcal{D})\mathcal{DP}} \\ &= (\Delta\mathcal{P} \cdot \frac{\rm d}{{\rm d}\mathcal{P}})[\mathcal{DP}(\boldsymbol{x}_{\rm cyc})] \cdot \mathcal{DP}^m(\boldsymbol{x}_{\rm cyc}) \cdot [\mathcal{DP}(\boldsymbol{x}_{\rm cyc})]^{-1} \\ &\quad + \mathcal{DP}(\boldsymbol{x}_{\rm cyc}) \cdot (\Delta\mathcal{P} \cdot \frac{\rm d}{{\rm d}\mathcal{P}})\mathcal{DP}^m(\boldsymbol{x}_{\rm cyc}) \cdot [\mathcal{DP}(\boldsymbol{x}_{\rm cyc})]^{-1} \\ &\quad + [\mathcal{DP}(\boldsymbol{x}_{\rm cyc})] \cdot \mathcal{DP}^m(\boldsymbol{x}_{\rm cyc}) \cdot \underbrace{(\Delta\mathcal{P} \cdot \frac{\rm d}{{\rm d}\mathcal{P}})[\mathcal{DP}(\boldsymbol{x}_{\rm cyc})]^{-1}}_{\text{utilize } (\mathbf{A}^{-1})'=\mathbf{A}^{-1}(-\mathbf{A}')\mathbf{A}^{-1}}, \end{aligned} \tag{C10}$$

which are, respectively, the counterparts of Eqs. (C2) and (C4) for mapping.

References

1. R. Rudnicki, Math. Meth. Appl. Sci. **27**, 723 (2004). https://doi.org/10.1002/mma.498
2. Y. Liang et al., Phys. Rev. Lett. **98**, 265004 (2007). https://doi.org/10.1103/PhysRevLett.98.265004
3. Y. Liang et al., Phys. Rev. Lett. **105**, 065001 (2010). https://doi.org/10.1103/PhysRevLett.105.065001
4. Y. Liang et al., Phys. Rev. Lett. **110**, 235002 (2013). https://doi.org/10.1103/PhysRevLett.110.235002
5. M. Jia et al., Nucl. Fusion **58**, 046015 (2018). https://doi.org/10.1088/1741-4326/aaaecc
6. M. Jia et al., Nucl. Fusion **61**, 106023 (2021). https://doi.org/10.1088/1741-4326/ac21f9
7. H. Frerichs et al., Phys. Rev. Lett. **125**, 155001 (2020). https://doi.org/10.1103/PhysRevLett.125.155001
8. R.K.W. Roeder et al., Phys. Plasmas **10**, 3796 (2003). https://doi.org/10.1063/1.1592515

9. T.E. Evans et al., Phys. Plasmas **9**, 4957 (2002). https://doi.org/10.1063/1.1521125
10. T.E. Evans et al., J. Phys: Conf. Ser. **7**, 174 (2005). https://doi.org/10.1088/1742-6596/7/1/015
11. T.E. Evans, Plasma Phys. Control. Fusion **57**, 123001 (2015). https://doi.org/10.1088/0741-3335/57/12/123001
12. E. Nardon et al., J. Nucl. Mater. **363**, 1071 (2007)
13. R. Balescu et al., Phys. Rev. E **58**, 951 (1998). https://doi.org/10.1103/PhysRevE.58.951
14. R. Balescu, Phys. Rev. E **58**, 3781 (1998). https://doi.org/10.1103/PhysRevE.58.3781
15. H. Frerichs et al., Phys. Plasmas **22**, 072508 (2015). https://doi.org/10.1063/1.4926524
16. M. Harsoula et al., Phys. Rev. E **97**, 022215 (2018). https://doi.org/10.1103/PhysRevE.97.022215
17. J.D. Meiss, Chaos **25**, pages 097602 (2015)https://doi.org/10.1063/1.4915831
18. E.E. Zotos, Nonlinear Dyn. **79**, 1665 (2015). https://doi.org/10.1007/s11071-014-1766-6
19. H.T. Moges et al., Phys. D **431**, 133120 (2022). https://doi.org/10.1016/j.physd.2021.133120
20. M.V. Falessi et al., J. Plasma Phys. **81**, 495810505 (2015). https://doi.org/10.1017/S0022377815000690
21. G. Di Giannatale et al., Phys. Plasmas **25**, 052306 (2018). https://doi.org/10.1063/1.5020163
22. F. Pegoraro et al., Plasma Phys. Control. Fusion **61**, 044003 (2019). https://doi.org/10.1088/1361-6587/ab03b5
23. M. Serra, L. Lemma, L. Giomi et al., Nat. Phys. **19**, 1355–1361 (2023)
24. F.L. Memarian et al., Phys. Rev. Lett. **132**, 228301 (2024). https://doi.org/10.1103/PhysRevLett.132.228301
25. J.D. Meiss, Phys. Rev. A **34**, 2375 (1986). https://doi.org/10.1103/PhysRevA.34.2375
26. O. Alus et al., Phys. Rev. E **90**, 062923 (2014). https://doi.org/10.1103/PhysRevE.90.062923
27. S. Abdullaev, *Magnetic Stochasticity in Magnetically Confined Fusion Plasmas: Chaos of Field Lines and Charged Particle Dynamics*, Springer Series on Atomic, Optical, and Plasma Physics (publisher Springer International Publishing, 2016)https://books.google.de/books?id=92RXvgAACAAJ
28. A.F. Haapala, K.C. Howell, Int. J. Bifurcat. Chaos **26**, 1630013 (2016). https://doi.org/10.1142/S0218127416300135
29. E. Trélat, Optim. Theory Appl. **154**, 712 (2012)
30. R. Chai et al., Prog. Aerosp. Sci. **109**, 100543 (2019). https://doi.org/10.1016/j.paerosci.2019.05.003
31. W. Wei, Y. Liang, Plasma Sci. Technol **25**, 095105 (2023). https://doi.org/10.1088/2058-6272/accbf5
32. B.A. Frigyik, S. Srivastava, M.R. Gupta, "An introduction to functional derivatives", Tech. Rep. UWEETR-2008-0001 (Department of Electrical Engineering, University of Washington, Seattle, WA, USA, 2008) https://vannevar.ece.uw.edu/techsite/papers/refer/UWEETR-2008-0001.html
33. D. Viswanath, Nonlinearity **16**, 1035 (2003). https://doi.org/10.1088/0951-7715/16/3/314
34. S.R. Hudson et al., Phys. Rev. Lett. **89**, 275003 (2002). https://doi.org/10.1103/PhysRevLett.89.275003
35. J. Loizu et al., J. Plasma Phys. **83**, 715830601 (2017). https://doi.org/10.1017/S0022377817000861
36. S. Zhou et al., Nucl. Fusion **62**, 106002 (2022). https://doi.org/10.1088/1741-4326/ac8439
37. A. Knieps et al., Nucl. Fusion **62**, 026011 (2021). https://doi.org/10.1088/1741-4326/ac3a18
38. C.S. Pitcher, P.C. Stangeby, Plasma Phys. Control. Fusion **39**, 779 (1997). https://doi.org/10.1088/0741-3335/39/6/001
39. V.A. Soukhanovskii, Plasma Phys. Control. Fusion **59**, 064005 (2017). https://doi.org/10.1088/1361-6587/aa6959
40. Y. Liang et al., Plasma Sci. Technol **24**, 124021 (2022). https://doi.org/10.1088/2058-6272/acaa8d